ISSN 2356-7171

Journal of Applied Chemistry

Volume No. 11

Issue No. 2

May - August 2025

ENRICHED PUBLICATIONS PVT.LTD

JE - 18,Gupta Colony, Khirki Extn,
Malviya Nagar, New Delhi - 110017.
E- Mail: info@enrichedpublication.com
Phone :- +91-8877340707

ISSN 2356-7171

Journal of Applied Chemistry

Aims and Scope

Journal of Applied Chemistry is a peer-reviewed, journal that publishes original research articles as well as review articles related to all aspects of applied chemistry. These includes the fields of analytical, inorganic, organic, physical and applied chemistry area. Review articles discussing specific areas of chemistry of current chemical importance are also published.

The journal welcomes publications of high quality papers on theoretical developments and practical applications in applied chemistry. Original research papers, state-of-the-art reviews, and high quality technical notes are invited for publications.

ISSN 2356-7171

Journal of Applied Chemistry

ISSN 2356-7171

Journal of Applied Chemistry

(Volume No. 11, Issue No. 2, May - August 2025)

Contents

ISSN 2356-7171

ANovel Tris(2-aminoethyl)amine Based Tripodal Ligand: Synthesis and Solution Coordination Studies with Trivalent Iron and Chromium

Minati Baral,1 Amit Gupta,1 Rifat Akbar,2 and Bikram K. Kanungo2
1Department of Chemistry, National Institute of Technology, Kurukshetra, Haryana 136119, India, 2Department of Chemistry, Sant Longowal Institute of Engineering and Technology, Longowal, Punjab 148106, India

ABSTRACT

Anoveltris(2-aminoethyl)amine (TREN) based tripodal ligand TRENOL (L) has been synthesized and characterized by elemental analysis and UV-VIS, IR, 1H, and 13C NMR spectroscopic methods. The coordination behaviour of the ligand with H+ and trivalent metal ions, Fe(III) and Cr(III), was investigated in aqueous medium at 0.1M KCl at 25 ± 1 C by potentiometric and spectrophotometric studies. Tripodal ligand showed seven protonation constants in the adopted pH range 2–11 and its electronic spectra exhibited three bands at 216, 323, and 423nm. Ligand formed various metal complex species of the type MLH5,MLH4, MLH3, MLH, and MLwith trivalent metal ions. The determined values of the formation constants (for ML species) of the ligand with Fe(III) and Cr(III) were 24.19 and 18.64, respectively. Molecular modeling studies revealed that the metal complexes formed distorted octahedral geometry. Besides, ligand showed fluorescence at 496nm when excited at 289nm. The fluorescence behaviour of the ligand in the presence of Fe(III) ions showed noticeable quenching in comparison to the other metal ions at physiological pH(7.4). So, as per the outcomes of the present study, TRENOL has the potential to be used as the iron detector in environmental, agricultural, and medical fields.

1. Introduction

Multifunctional compounds such as polyphenols are highly abundantinnaturalproductslikepine,grape,andwitchhazel products. They are broadly beneficial for human health as they are found highly active and protective for red blood cells from free radical induced hemolysis. However, polyphenols serve as double-edged sword due to their both antioxidative and prooxidative properties. They are capable of scavenging freeradicalsandinothercasescanserveasreactiveoxygen species[1]and,hence,canbeexploredeitherasaneffective antioxidant or as a cytotoxic agent in various hyperproliferative diseases. Besides biological studies, polyphenols based Schiff bases can be designed to demonstrate the coordination behaviourof thesebiologicalpotentagentswithmetal ions which may further provide additive properties to this class of compounds. Schiff bases are much prevailing compounds in coordination chemistry due to their capability of forming stable complexeswithmetalions[2].Theyareknownfortheir high selectivity and sensitivity with specific metal ions and so they are useful in potentiometric sensing and heterogeneous catalytic processes [3]. Despite their high significance against potent pathogens only limited data is available in the field of metal

complexation. This less investigated area can be studied forbetter understandingofelectronic,molecular,and spectral behaviour of polyphenols based Schiff bases and their metal complexes. Such studies provide a strong ground for the development of novel sensor or agents with wider applications.

Iron overload transfusion therapy is generally used to cure such a metal poisoning, which includes administration of iron chelating agents [4]. Potential chelators are biologically available and are featured by lesser toxicity, high selectivity towards iron, and forming stable complex upon binding with it. In these aspects, low molecular weight naturally occurring biomolecules, siderophores, have capability to bind with iron with high affinity and specificity. Nowadays, iron uptake by those biomolecules is serving as a novel platform for various applications, based on ironuptakemechanismsuchas drugdelivery system[5, 6], detection of microorganisms [7, 8], and capture and accumulation of actinide elements [9–11]. In order to put some appropriate solution, synthesis of novel molecules is required which may be considered against intoxication of aforesaid metals in the biological systems and may also be used for developing some sought probes for the detection of these metals in trace quantity if present in the surrounding environment.

Moreover, for developing novel chelators, it is necessary to coverthestructural aspects of natural occurring molecules suchassiderophores.Duringtheworldwidesearchforpotential siderophore mimic chelators, it has been observed that several research groups have developed different strategies for synthesis of such tripodal chelating agents. Much effort has been channeled into the synthesis of catechols [12] and hydroxamates [13–16] with typical examples (model chelators) being enterobactin and desferrioxamine, respectively. The most important work was carried out by the Raymondgroupwhohavereportednumerouscatecholate [17] and hydroxypyridone ligands [18, 19]. A number of synthetic analogues have been prepared which retain the high affinity for iron(III) and with other metal ions, typical of enterobactin, and yet are more stable under biological conditions, for instance, the tripodal molecular Mecam [20]. Mecam is the structural analogue of enterobactin and has three catechol binding units: the catecholamide groups are appended to 1,3,5-triaminomethyl benzene rather than to the tri-L-serine ligand backbone of enterobactin. Many derivatives of Mecam have been reported [12, 21–23]. The thermodynamics, kinetics, and electrochemical studies along with biological evaluation of these ligands are reported in numerous articles and reviews [24, 25]. Attempts have been made to synthesize lipophilic tripodal hexadentate ligand, where three bidentate moieties are attached to core by stable arms such as carbon chain and ether linkers [26, 27] containing C-pivot, tris(aminomethyl)ethane (tame) as center unit. Another important aspect is the ring strain due to the rigidity of the benzene ring, as it could be expected if the sp2 hybridized atoms of benzene ring are

replaced with sp3 hybridized systems like cyclohexane ring, the resulting tripod system would be more flexible and ring strain will be less comparedtoMecamandcomplexeswouldbethermodynamicallymorestable[28];designofsuchtripodalsystems by replacing benzene ring with a cyclohexane ring has been reported [29–33].

T houghmany tripodal siderophoremimics containing phenolate, catecholate, and other binding units have been reported, very few pyrogallol type multidentate chelators have been reported [34] and detailed studies have been reported. Keeping in view of the above, a polyhydroxy tripodal ligand incorporated with azomethine spacer has been synthesized from TREN and 2,3,4-trihydroxybenzaldehyde and its coordination behaviour towards Fe(III) and Cr(III) is studied.

2. Experimental

2.1. Chemicals and Solvents. Reagents for synthesis pur pose of tris(2-aminoethyl)amine (TREN), 2,3,4-trihydroxybenzaldehyde, and so forth were purchased from SigmaAldrich and used without further purification. Analytical grade solvents tetrahydrofuran, ethanol, and others were purchased from Loba Chemie Pvt. Ltd. and Fisher Scientific. Before using, solvents were dried over suitable drying reagents. Solvents were freshly distilled over appropriate drying agents following standard procedures.2.2. Physical Measurements. Melting points of the com pounds were determined on Microsil apparatus. Elemental analysis (CHN) was performed on Euro EA 3000, 60Hz1200W elemental analyzer. For FT-IR analyses, the sample was carefully mixed in homogenous manner in KBr in 1:100 by weight and a fine pellet was prepared under pressure. T he FT-IR spectrum of the compound was taken under transmissionmodewithPerkin-ElmerFT-IRspectrometerin mid-range region (4000–400)cm−1.The1Hand13CNMR spectra of the ligand TRENOL were taken in d6 dmso using BrukerAvanceII400NMRspectrometer.Thechemicalshifts were quantified in alues (ppm). Tetramethylsilane was used as an internal reference. To avoid solubility problem, the compound was converted into its hydrochloric salt and dissolved in millipore grade deionized water. Ionic strength of the solution was adjusted with 0.1M KCl. All the stock solutions were prepared in millipore grade deionized water. For weighing appropriate amount, high precision weighing balance CAS-CAUW220D was used (up to level of four digits). The exact concentration of KOH (0.1M) was determined potentiometrically using 0.1M solution of oxalic acid as primary standards and then exact strength of HCl (0.1N) was determined by the same method using standardized KOH. All the solutions were prepared with millipore grade deionized water immediately before use, which was deoxygenated and flushed continuously with grade I N2 gas to CO2 and O2. All measurements were carried out at 25 ±1 C maintained by using thermostat.

2.3. Synthesis and Characterization. 0.146g (1.0mmol) of TRENwasaddedgraduallytothestirringsolutionof0.4673g (3.0 mmol)2,3,4-trihydroxy-benzaldehydedissolvedinabsolute ethanol (30.0mL) under nitrogen gas atmosphere for 12 h at room temperature (Figure 1). The obtained yellowishorange precipitates were filtered and subjected to crystallization in methanol/tetrahydrofuran solvent mixture. The yellow colour solid (TRENOL) with yield 80% and melting point 186–188 C was characterized by elementary analysis and different spectroscopic techniques. Elemental analysis of carbon ©, hydrogen (H), and nitrogen (N) in percentage was found to be C 57.83, H 5.62, N 10.12; calculated ($C_{27}H_{30}N_4O_9$), C 58.54, H 5.52, N 10.14. IR (KBr) ν_{max}/cm^{-1}: 3365 (O-H), 2925 (N-H amide), 1595 (-C=N-), 1352 (oop, C-O-H cm^{-1}); ^1H NMR spectra δ (400 MHz, dmso), δ (ppm): 2.7 (t, 6H, J = 8.1, -CH_2-), 2.9 (t, 6H, J = 8.1 -CH_2-), 6.0–7.0 (m, 6H, J = 8.0, Ar-H), 9.7 (s, 3H, -N=CH-), 7.0 (s, 3H, -OH), 7.9 (s, 3H, -OH), 8.2 (s, 3H, -OH); ^{13}C NMR spectra δ

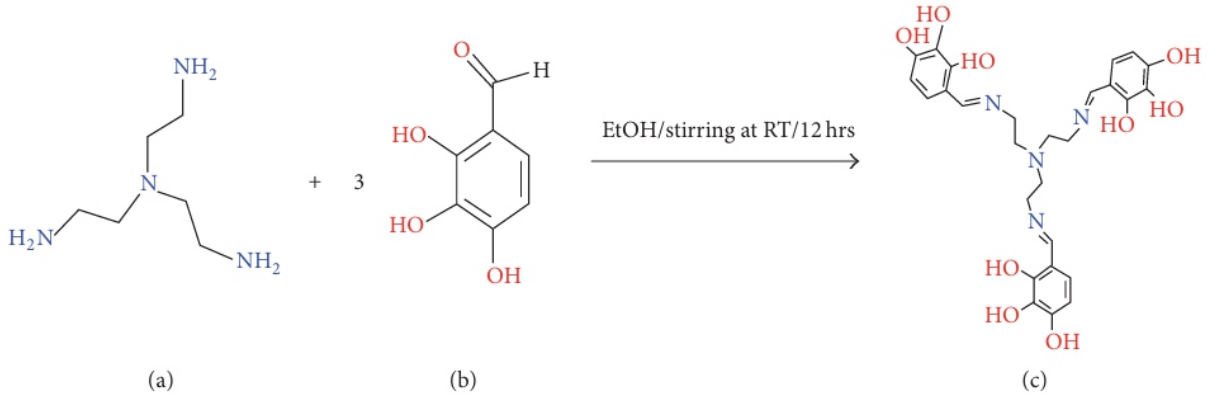

Figure 1: Scheme for synthesis of tripodal Schiff base. (a) TREN; (b) 2,3,4-trihydroxy-benzaldehyde; (c) TRENOL.

(400 MHz, dmso): δ = 106–158 (18C, -Ar), 164 (3C, -N=CH-), 55 (3C, $-CH_2$), 53 (3C, $-CH_2$).

2.4. Potentiometric Titration. Determination of protonation constants (log K) of the ligand and its formation constants (log β) with two trivalent metal ions, Fe(III) and Cr(III), was done by potentiometry and spectrophotometry methods. The potentiometric titrations were carried out on HACH Sension-2 potentiometer using glass electrode and pH was recorded as $-\log[H^+]$. The standard method was used for electrode calibration in suitable buffers of pH 4 and pH 7 [35]. All the titrations were carried out using auto pipette with least count 10 μM and capacity 1.0 mL. In potentiometric method final concentration 1×10^{-5} M was fixed for both ligands and metal ions. The ligand solution, in the absence and presence of metal ions, was titrated against 0.1 M KOH at μ = 0.1 M KCl at 25 ± 1°C in pH range 2–11 and adequate time was given for the attainment of the equilibrium to give a stable pH reading. Hyperquad 2006 nonlinear least square program was used for the refinement of potentiometric data [36]. During the titration with increasing pH, the species formed were observed using the simulation program HYSS 2009 [37].

2.5. Spectrophotometric and Fluorescence Studies. Spectrophotometric titrations were carried out under the same conditions by keeping the final ligand concentration 2×10^{-5} M. During titration after each addition of base KOH, sufficient time was allowed for establishment of the equilibrium and a small aliquot of the solution was taken in to the cuvette (1 cm, path length) to take the spectra. The computer software HypSpec [38] was used for the determination of protonation constants of the ligand and formation constants of the metal complexes with Fe(III) and Cr(III).

The fluorescence study of the ligand was conducted on Agilent Fluorescence Spectrophotometer. The emission spectra of the ligand in the absence and presence of metal ions in 1 : 1 M-L stoichiometry were studied with λ_{ex} = 289 nm in the same method under similar conditions as mentioned for spectrophotometric titrations in pH range 2–9. Also, the effect of increasing concentration of the Fe(III) (2 to 1000 μM) on the fluorescence intensity of the tripodal ligand (20 μM) was investigated at pH 7.4 ± 0.1 using HEPES buffer. In a similar way fluorescence behaviour of the ligand was also studied in the presence of metal ion (Na^+, K^+, Ca^{2+}, Mg^{2+}, Zn^{2+}, Co^{2+}, Pb^{2+}, Cu^{2+}, Al^{3+}, and Cr^{3+}). Moreover, the detection limit was calculated for the iron on the basis of fluorescence titration at pH 7.4 according to the definition by IUPAC, that is, 3.3 ∗ SD/m, where "SD" is the standard deviation of the fluorescence intensity of the blank (ligand only) and "m" is the slope of the calibration curve constructed between fluorescence intensity of ligand (20 μM) at 490 nm and the concentration of Fe(III) in μM. For determining the SD, the fluorescence emission spectra of the blank were measured 10 times [39].

Table 1: Stepwise protonation constants (log K) of the TRENOL (L), at 25 ± 1°C and μ = 0.1 M KCl.

Reaction	log K	Protonation sites
$L + H \rightleftharpoons LH$	10.02 ± 0.04	$-O^-$ (aromatic)
$LH + H \rightleftharpoons LH_2$	8.21 ± 0.05	$-O^-$ (aromatic)
$LH_2 + H \rightleftharpoons LH_3$	7.83 ± 0.03	$-O^-$ (aromatic)
$LH_3 + H \rightleftharpoons LH_4$	7.45 ± 0.06	-N (apical)
$LH_4 + H \rightleftharpoons LH_5$	2.51 ± 0.03	-N (imine)
$LH_5 + H \rightleftharpoons LH_6$	1.82 ± 0.04	-N (imine)
$LH_6 + H \rightleftharpoons LH_7$	1.24 ± 0.05	-N (imine)
$L \rightleftharpoons LH_{-1} + H^+$	−8.36 ± 0.05	—
$L \rightleftharpoons LH_{-2} + 2H^+$	−8.77 ± 0.03	—
$L \rightleftharpoons LH_{-3} + 3H^+$	−9.39 ± 0.06	—
$L \rightleftharpoons LH_{-4} + 4H^+$	−10.80 ± 0.04	—
$L \rightleftharpoons LH_{-5} + 5H^+$	−11.00 ± 0.03	—
$L \rightleftharpoons LH_{-6} + 6H^+$	−11.16 ± 0.03	—

2.6. Molecular Modeling and Computational Methods. All computational simulations were done on a Pentium Dual-Core 3.20 GHz machine in Windows XP environment. The initial structures of the ligand and their metal complexes for optimization were manually drawn using Symyx Draw. The initial geometry optimization of the ligands, its protonated and deprotonated species obtained in solution, and its metal complexes leading to minimum strain energy was achieved through molecular mechanics calculation using MM+ force field by software HyperChem version 7.5 [40]. The obtained structure of the ligand was reoptimized semiempirically using PM3, self-consistent fields (SCF) method [41]. The steepest descent method followed by Polak-Ribiere method with convergence limit of 0.0001 Kcal/mol and RMS gradient of 0.001 Kcal/mol was used to get geometry optimizations.

3. Results and Discussion

3.1. Synthesis and Characterization of TRENOL. A yellowish-orange colour product (TRENOL) with reasonable yield (80%) obtained from single condensation of TREN and 2,3,4-trihydroxybenzaldehyde is stable to air and has melting point 186–188°C. The compound was completely soluble in dmso and partially soluble in ethanol but highly insoluble in dichloromethane, ether, acetonitrile, and so forth. Structural characterization of the tripodal ligand was done through FT-IR, ^{1}H, ^{13}C NMR, and CHN analysis. The FT-IR spectrum of the ligand showing a sharp peak at 1595 cm^{-1} is due to ν(-C=N-) that ensured amine-aldehyde condensation and formation of the Schiff base. The strong band near 3365 cm^{-1} was obtained due to stretching vibration of the -OH group,

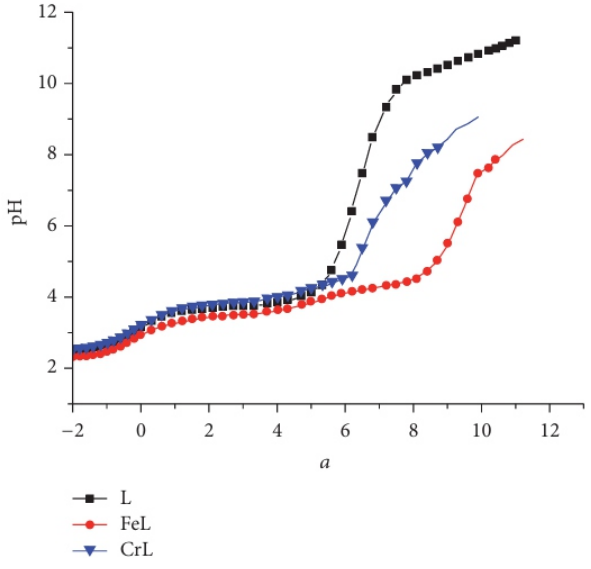

that is, ν(-OH). Another peak obtained at 2925 cm^{-1} was assigned to the ν(-NH) of the amide linkage. Theoretical IR values were calculated by using semiempirical/PM6 parameters which showed pattern of the peaks similar to that of the experimental IR. The ^{1}H NMR spectra of the ligand showed peaks at 2.7 ppm and 2.9 ppm which correspond to the methylene group (-CH_2) present in the vicinity of bridgehead nitrogen and imine groups, respectively. The signal that appeared at 9.7 ppm was assigned to the -HC= group and presence of aromatic ring was confirmed from a multiplet found in the range 6.0–7.0 ppm. Singlets obtained between 7.0 and 8.2 ppm correspond to the -OH groups of the aromatic ring [42]. In ^{13}C NMR spectra, the peak obtained at 164 ppm confirmed the presence of imine group in the ligand and signals near 53 and 55 ppm ensured the presence of methylene groups. The aromatic ring C –atoms appeared in the range 106–158 ppm.

3.2. Determination of Protonation Constants. The protonation constants of the ligand were determined by potentiometric and spectrophotometric studies. Due to solubility limitation of the ligand in aqueous medium its hydrochloric salt was prepared prior to investigation. The neutral form of the ligand is considered as LH_3 and the fully protonated form is considered as $(LH_7)^{4+}$. The obtained values in the pH range 2–11 are defined by the following equations:

$$[LH_{n-1}] + [H] \rightleftharpoons LH_n,$$
$$K_{1n} = \frac{[LH_n]}{[LH_{n-1}]\,[H]}. \quad (1)$$

Analysis of the curve (Figure 2) using Hyperquad offered seven protonation constants (log K) as shown in Table 1.

Although ligand TRENOL has thirteen dissociable protons, only seven protons could be deprotonated in the adopted experimental pH range 2–11. The first three protonation constants were attributed to the ortho -OH groups of the aromatic ring. However, deprotonation of meta and para -OH groups could not be obtained due to the presence of intramolecular H-bonding and enhanced electron density in the ring which triggers after deprotonation of ortho hydroxy groups. The fourth protonation constant pertained to the apical nitrogen and the remaining three belong to azomethine groups. The obtained protonation constants for -OH groups (aromatic ring), apical "N," and -C=N- groups were in good agreement with the existing literature [42, 43]. The experimental curve did not give complete match with the theoretical curve at higher pH (i.e., >8.5) by only considering seven protonation constants, but by inclusion of six hydrolyzed species, namely, LH_{-1}, LH_{-2}, LH_{-3}, LH_{-4}, LH_{-5}, and LH_{-6} in the model, the refinement process gave best fit to the experimental curve.

Figure 2: Potentiometric titration curves between pH and "a" (moles of base added per mole of the ligand) in the presence of metal ions, Fe(III), and Cr(III) in 1 : 1 molar ratio; [M] = [L] = 1×10^{-5} M at μ = 0.1 M KCl and T = 25 ± 1°C.

Also, as evident from the literature, Schiff bases are less stable in an alkaline medium and undergo hydrolysis [44]. The existence of various deprotonated and hydrolyzed species was pH dependent and formation of such species at different pH is evident from the species distribution diagram (Figure 3).

Protonation constants of the ligand were also obtained from the spectrophotometric technique. Analysis of spectrophotometric data obtained in pH range 2–9 also confirmed the seven protonation constants of the ligand and all were found in good agreement with the potentiometric data (Figure 4). Appearance of new absorption band and enhancement in the intensity implicate the deprotonation of the chromophoric groups. The electronic spectra of the ligand showed three bands at 216, 289, and 423 nm at low pH ~2 and were assigned to $\pi \rightarrow \pi^*$ (former two) and $n \rightarrow \pi^*$ (latter one) transitions.

No significant change was found in the spectra of the ligand in the pH range 2–6, but pH beyond this causes

Table 2: Formation constants (log β) of M-L complexes, where M = Fe(III) and Cr(III), A = potentiometry, and B = spectrophotometry.

	Fe(III)		Cr(III)	
	A	B	A	B
$\frac{[ML]}{[M][L]}$	24.01 ± 0.03	24.21 ± 0.04	18.64 ± 0.07	18.75 ± 0.06
$\frac{[MLH]}{[M][L][H]}$	30.01 ± 0.05	30.56 ± 0.04	26.52 ± 0.03	26.69 ± 0.02
$\frac{[MLH_3]}{[M][L][H]^3}$	39.56 ± 0.04	39.88 ± 0.03	36.75 ± 0.04	36.91 ± 0.05
$\frac{[MLH_4]}{[M][L][H]^4}$	43.56 ± 0.06	43.75 ± 0.06	40.79 ± 0.06	40.98 ± 0.04
$\frac{[MLH_5]}{[M][L][H]^5}$	45.43 ± 0.06	45.75 ± 0.05	44.10 ± 0.03	44.45 ± 0.02

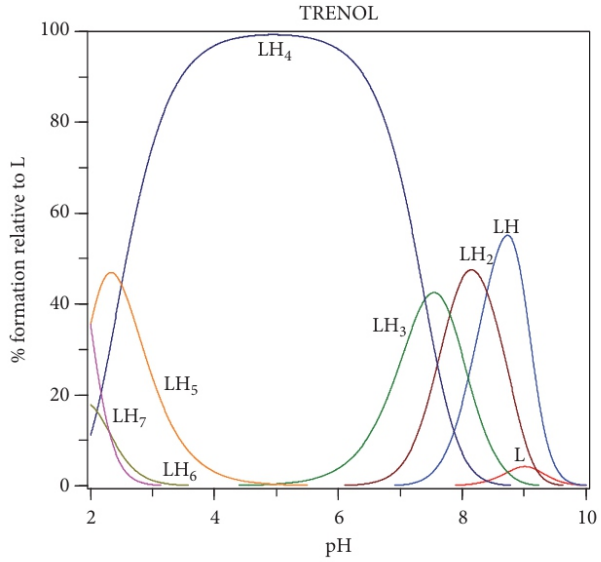

Figure 3: pH dependent species distribution curve of the ligand (TRENOL).

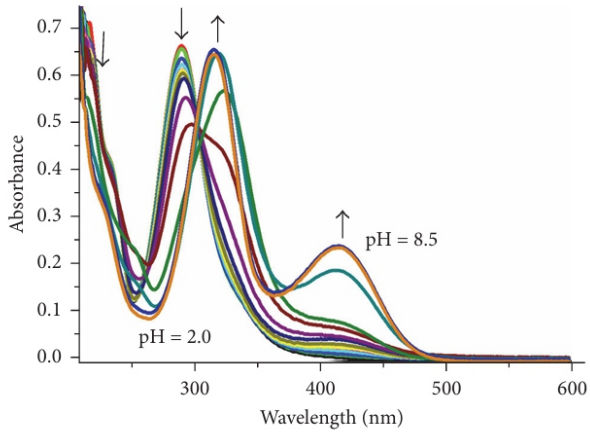

Figure 4: Electronic spectra of ligand as a function of pH (2.0–9.0) during spectrophotometric titration; [L] = 2×10^{-5} M and $T = 25 \pm 1^{\circ}$C.

shifting of bands from 289 to 323 nm corresponding to deprotonation of the aromatic ortho -OH groups. The shifting of bands towards longer wavelength is justified by the fact that on deprotonation the stabilization of π^* state by charge delocalization occurs which reduces the energy of transition and also influences the absorption intensity at 423 nm due to the presence of conjugation between azomethine group and aromatic ring.

3.3. Metal Complexation Studies. The complexation behaviour of the ligand with Fe(III) was investigated in a pH range 2–9 using equimolar solution of ligand and metal ions and also with another trivalent metal ion Cr(III) for comparative studies. The metal-ligand potentiometric titration curves show the deviation from the ligand only at the lower pH region which implicates complexation of the ligand with the metal ions (Figure 2). Several models were considered to get the best fit through the refinement process. The complete agreement of the experimental and theoretical curves was obtained by considering the model as given in Table 2.

In Fe(III)-L metal complex, no major shift in the absorption bands was obtained in the pH range from 2.0 to 4.0, which supported the deprotonation of nonchromophoric groups of the ligand (i.e., azomethine groups). On increasing the pH beyond the aforesaid range, one of the absorption bands ($\pi \rightarrow \pi^*$) for aromatic ring at 289 nm experienced red shift (317 nm) with concomitant rise in absorption intensity implicating the deprotonation of -OH groups on aromatic ring while appearance of a low intensity band at 423 nm in comparison to the ligand shows the complexation of the ligand with the metal ions. Similarity in spectral changes with Cr(III) indicates similar mode of complexation of the chelator. Electronic spectra of the ligand with Fe(III) and Cr(III) were recorded between 200 and 600 nm as shown in Figure 5.

Analysis of the species distribution diagram of metal-ligand complexes as a function of pH showed that Fe(III) and Cr(III) coordinated to the ligand at low pH (~2.0) through imine group with the formation of MLH_5 type species (Figure 6). Coordination of weakly basic imine groups with metal ions at low pH is well supported by literature [11]. In the pH range 2–4 the deprotonated species, MLH_4, was 88% for Fe(III) and 50% for Cr(III). With subsequent increase in the pH (4 to 8) the iron complexes MLH_3 (60%),

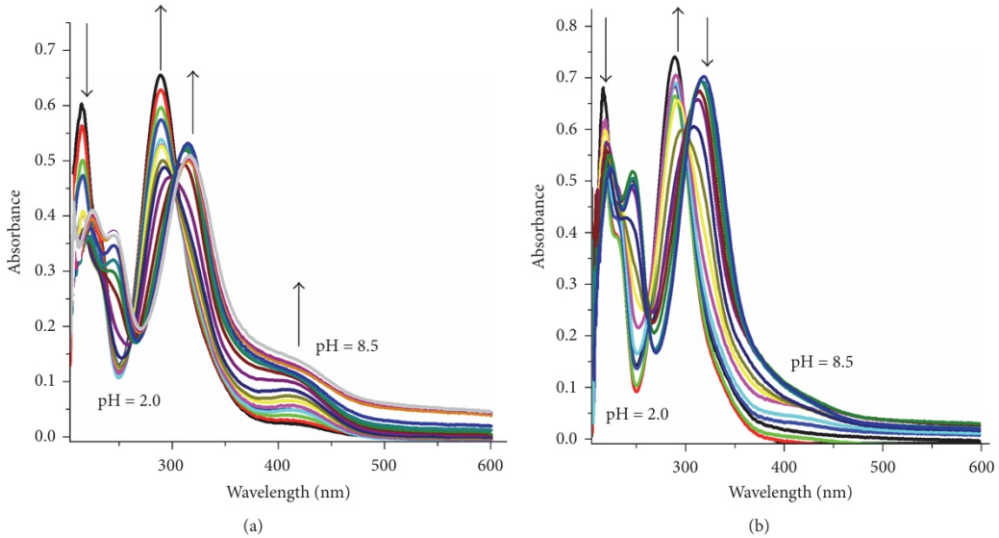

FIGURE 5: Electronic spectra of L as a function of pH during spectrophotometric titration with [M] = 2×10^{-5} M where M = (a) Fe(III) and (b) Cr(III); [L] = 2×10^{-5} M at μ = 0.1 M KCl and T = 25 ± 1°C.

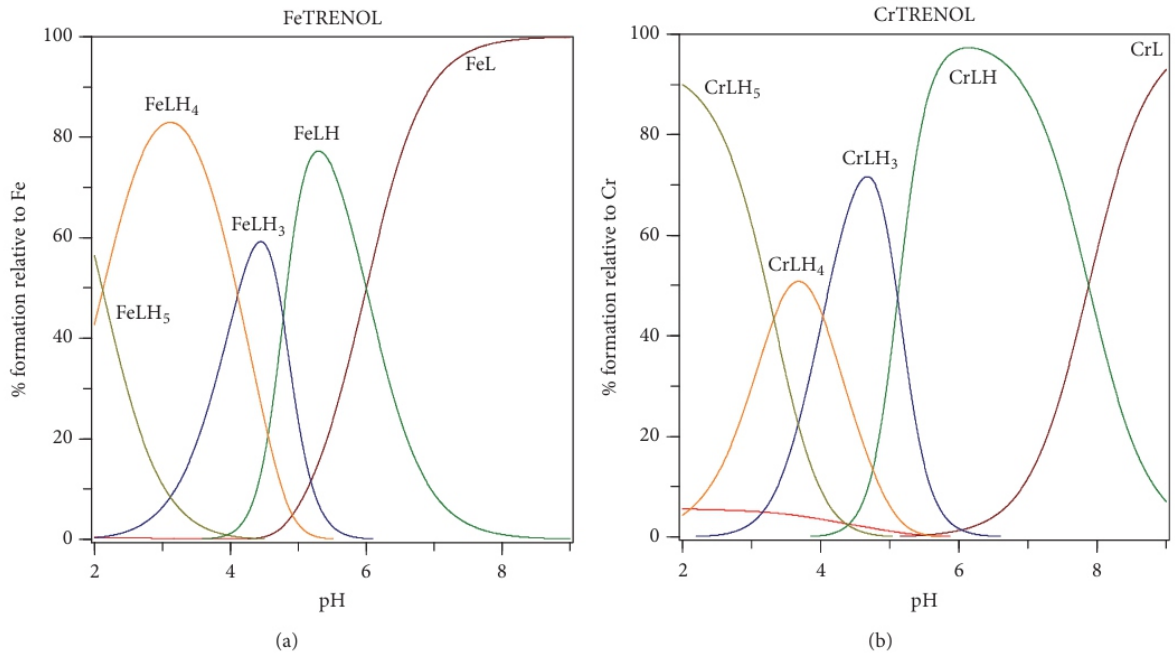

FIGURE 6: pH dependent distribution curves of the species of metal-ligand complexes (a) Fe(III)-L and (b) Cr(III)-L.

MLH (78%), and ML (100%) were found in the solution due to the deprotonation of aromatic hydroxy groups of the ligand. Similarly, in pH range 4–8, Cr(III) formed MLH_3 (80%), MLH (91%), and ML (92%) species in the solution. The deprotonation of the ligand in the presence of metal ions at lower pH range (4 to 6 for Fe(III) and 4.2 to 7.2 for Cr(III)) in comparison to the ligand alone (pH 6 to 8) was justified by the higher preference of the metal ions for the donor atoms of the ligand (O and N) when compared to protons. However, the potentiometric data of the ligand showed that, in pH range 4–6, deprotonation of the apical nitrogen occurred which might be overlapped by the deprotonation of chromophoric group in the presence of metal ions. The prediction was also well supported through the analysis of electronic absorption spectra of the metal complexes in the same region. Such deviation in the deprotonation behaviour

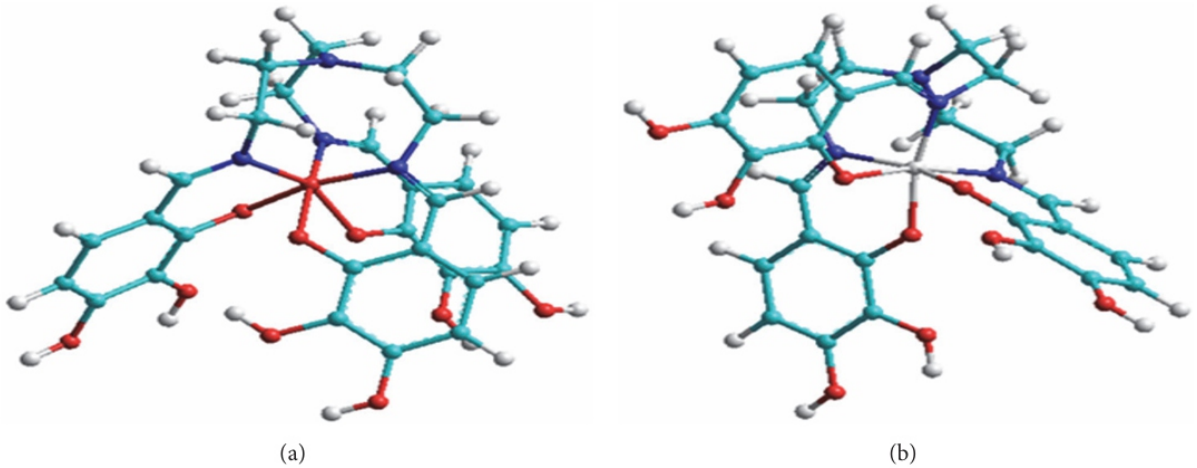

FIGURE 7: Lowest energy structures of M-L complexes (a) Fe(III)-L and (b) Cr(III)-L.

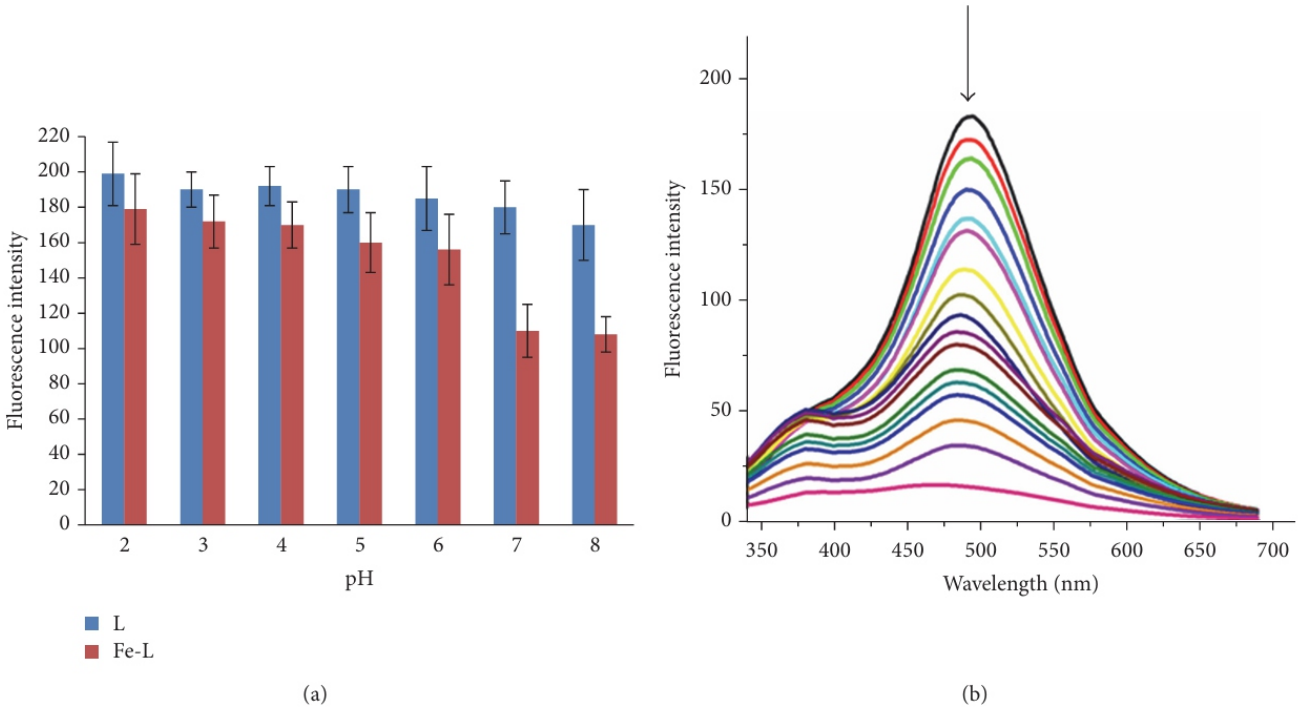

FIGURE 8: (a) pH dependent fluorescence intensities with standard deviations of ligand (L) and Fe(III)-L. (b) Fluorescence spectra of the ligand with increasing concentration of Fe(III), where [L] = 20 μM and [Fe(III)] = 2 to 1000 μM (from top to bottom) at pH = 7.4, λ_{ex} = 289 nm, and λ_{em} = 496 nm.

of the apical nitrogen has also been discussed in the literature with several different concepts according to their ligand structures [45].

In order to depict the coordination mode of the ligand with metal ions, molecular modeling studies were carried out for all the formed species of metal-ligand complexes (MLH_5, MLH_4, MLH_3, MLH, and ML) using molecular mechanics with MM+ force field [39] followed by optimization by semiempirical PM3 parameters [40]. Among these species, M-L type species was found to be the most stable species based on the least strain minimum energy structures (Figure 7). Moreover, bond length and bond angles for the M-L type complexes were calculated and it was found that the metal complexes possessed distorted octahedral geometry.

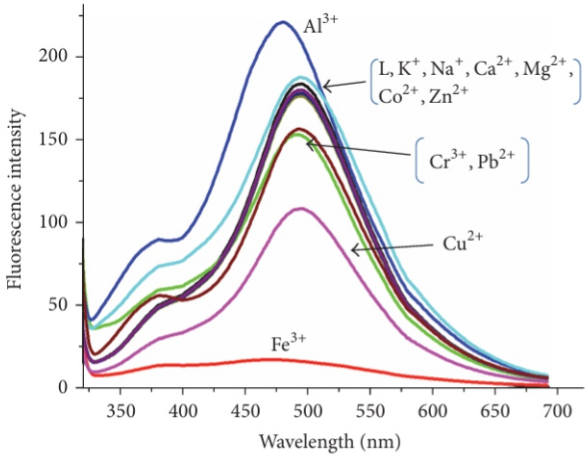

FIGURE 9: Fluorescence spectra of TRENOL in presence of different metal ions: [L] = 20 μM, [M] = 1000 μM at λ_{ex} = 289 nm, and pH = 7.4.

3.4. Studies of Photophysical Properties. The fluorescence behaviour of the ligand was investigated in the wavelength range 350–700 nm under similar conditions as done in spectrophotometric method. The ligand exhibited fluorescence at 496 nm with slit width 20 nm and λ_{ex} = 289 nm. Presence of transition metal ions in the vicinity of fluorophore changes its photophysical properties through modulated oxidation potential of the donor group leading to fluorescence enhancement or quenching [46, 47]. The fluorescence behaviour of the ligand was initially studied in the presence of Fe(III) with variation in pH, given in Figure 8(a). TRENOL exhibited maximum quenching between pH 7 and pH 8 after which precipitation occurred. The fluorescence behaviour of the ligand was also studied at different concentrations of Fe(III)

Acknowledgments

The authors would like to thank the Department of Chemistry, National Institute of Technology, Kurukshetra, for providing the facilities.

References

[1] S. Touriño, D. Lizárraga, A. Carreras et al., "Antioxidant/prooxidant effects of bioactive polyphenolics," *Electronic Journal of Environmental, Agricultural and Food Chemistry*, vol. 7, no. 8, pp. 3348–3352, 2008.

[2] A. M. Abu-Dief and I. M. A. Mohamed, "A review on versatile applications of transition metal complexes incorporating Schiff bases," *Beni-Suef University Journal of Basic and Applied Sciences*, vol. 4, no. 2, pp. 119–133, 2015.

[3] M. A. Ashraf, K. Mahmood, and A. Wajid, "Synthesis, characterization and biological activity of Schiff bases," in *Proceedings of the International Conference on Chemistry and Chemical Process (ICCCP '11)*, vol. 53, pp. 1–7, Bangkok, Thailand, 2011.

at physiological pH (Figure 8(b)). The detection limit of the Fe(III) was found to be around 1.4×10^{-5} M.

To explore more on the ligand's selectivity in fluorescence sensing, different metal ions such as Na^{+}, K^{+}, Ca^{2+}, Mg^{2+}, Zn^{2+}, Co^{2+}, Pb^{2+}, Cu^{2+}, Al^{3+}, and Cr^{3+} were taken for the study. Figure 9 shows fluorescence quenching in the ligand with Fe(III) as compared to other metal ions used. The quenching is maximum (9-fold compared to ligand alone) with [Fe(III)] = 1000 μM at physiological pH, whereas none of the above-mentioned metals showed any significant effect. However, the ligand shows little quenching (~1.5-fold) in presence of Cu(II) and negligible quenching (~0.5-fold) with Pb(II) and Cr(III).

4. Conclusions

In summary a novel tris(2-aminoethyl)amine based tripodal ligand, TRENOL with seven protonation constants in pH range 2–11, was developed that served as a potential Fe(III) binding chelator. The preorganized structure of the ligand offered a favorable environment for a strong encapsulation of Fe(III) with high binding constant value (ML, $\log\beta$ = 24.01) as compared to Cr(III). Moreover, the tripodal chelator showed fluorescence through assisted ESIPT mechanism at 490 nm. The fluorescence behaviour of the ligand exhibited maximum quenching in the presence of Fe(III) metal ions at physiological pH in comparison to other biological relevant metal ions and limit of detection for the Fe(III) was found to be 1.4×10^{-5} M. Therefore, the ligand (L) may be cited as an alternate for the detection of iron for further modification to develop a better potent fluorescence sensor.

Competing Interests

The authors declare that they have no competing interests.

[4] S. L. Byrne, D. Krishnamurthy, and M. Wessling-Resnick, "Pharmacology of iron transport," *Annual Review of Pharmacology and Toxicology*, vol. 53, pp. 17–36, 2013.

[5] G. Winkle Mann and C. J. Carrano, *Transition Metals in Microbial Metabolism*, Harwood Academic, Amsterdam, The Netherlands, 1997.

[6] G. Winkle Mann, *Handbook of Microbial Iron Chelates*, CRC Press, New York, NY, USA, 1998.

[7] C. R. Lloyd, F. C. Cleary, H.-Y. Kim et al., "Is what you eat and drink safe? Detection and identification of microbial contamination in foods and water," *Proceedings of the IEEE*, vol. 91, no. 6, pp. 908–914, 2003.

[8] H. Y. Mason, C. Llyod, M. Dice, R. Cinclair, and W. Ellis Jr., "Taxonomic identification of microorganisms by capture and intrinsic fluorescence detection," *Biosensors and Bioelectronics*, vol. 18, no. 5-6, pp. 521–527, 2003.

[9] S. G. John, C. E. Ruggiero, L. E. Hersman, C.-S. Tung, and M. P. Neu, "Siderophore mediated plutonium accumulation by *Microbacterium flavescens* (JG-9)," *Environmental Science and Technology*, vol. 35, no. 14, pp. 2942–2948, 2001.

[10] C. E. Ruggiero, J. H. Matonic, S. D. Reilly, and M. P. Neu, "Dissolution of plutonium(IV) hydroxide by desferrioxamine siderophores and simple organic chelators," *Inorganic Chemistry*, vol. 41, no. 14, pp. 3593–3595, 2002.

[11] T. Yoshida, T. Ozaki, T. Ohnuki, and A. J. Francis, "Adsorption of Th (IV) and Pu (IV) on the surface of pseudomonas fluorescens and bacillus subtilis in the presence of desferrioxamine siderophore," *Journal of Nuclear and Radiochemical Sciences*, vol. 6, no. 1, pp. 77–80, 2005.

[12] S. J. Rodgers, C. W. Lee, C. Y. Ng, and K. N. Raymond, "Ferric ion sequestering agents. 15. Synthesis, solution chemistry, and electrochemistry of a new cationic analog of enterobactin," *Inorganic Chemistry*, vol. 26, no. 10, pp. 1622–1625, 1987.

[13] M. J. Miller, "Syntheses and therapeutic potential of hydroxamic acid based siderophores and analogues," *Chemical Reviews*, vol. 89, no. 7, pp. 1563–1579, 1989.

[14] R. J. Bergeron, J. Wiegand, J. S. Mcmanis, and P. T. Perumal, "Synthesis and biological evaluation of hydroxamate-based iron chelators," *Journal of Medicinal Chemistry*, vol. 34, no. 11, pp. 3182–3187, 1991.

[15] A. L. Crumbliss, "Iron bioavailability and the coordination chemistry of hydroxamic acids," *Coordination Chemistry Reviews*, vol. 105, pp. 155–179, 1990.

[16] J. H. Crosa, "Genetics and molecular biology of siderophore-mediated iron transport in bacteria," *Microbiology and Molecular Biology Reviews*, vol. 53, no. 4, pp. 517–530, 1989.

[17] J. B. Porter, "A risk-benefit assessment of iron-chelation therapy," *Drug Safety*, vol. 17, no. 6, pp. 407–421, 1997.

[18] M. Y. Moridani, G. S. Tilbrook, H. H. Khodr, and R. C. Hider, "Synthesis and physicochemical assessment of novel 2-substituted 3-hydroxypyridin-4-ones, novel iron chelators," *Journal of Pharmacy and Pharmacology*, vol. 54, no. 3, pp. 349–364, 2002.

[19] M. A. Santos, S. M. Marques, and S. Chaves, "Hydroxypyridinones as 'privileged' chelating structures for the design of medicinal drugs," *Coordination Chemistry Reviews*, vol. 256, no. 1-2, pp. 240–259, 2012.

[20] M. M. Meijler, R. Arad-Yellin, Z. I. Cabantchik, and A. Shanzer, "Synthesis and evaluation of iron chelators with masked hydrophilic moieties," *Journal of the American Chemical Society*, vol. 124, no. 43, pp. 12666–12667, 2002.

Fe(III)," *Spectrochimica Acta—Part A: Molecular and Biomolecular Spectroscopy*, vol. 74, no. 2, pp. 544–552, 2009.

[31] S. K. Sahoo, M. Baral, and B. K. Kanungo, "Tripodal amine catechol ligands: a fascinating class of chelators for aluminium(III)," *Journal of Inorganic Biochemistry*, vol. 102, no. 8, pp. 1581–1588, 2008.

[32] S. K. Sahoo, M. Baral, and B. K. Kanungo, "Potentiometric, spectrophotometric, theoretical studies and binding properties of a novel tripodal polycatechol-amine ligand with lanthanide(III) ions," *Polyhedron*, vol. 25, no. 3, pp. 722–736, 2006.

[33] R. K. Bera, M. Baral, S. K. Sahoo, and B. K. Kanungo, "Spectroscopic, potentiometric and theoretical studies of novel iminophenolate chelators for Fe(III)," *Spectrochimica Acta—Part A: Molecular and Biomolecular Spectroscopy*, vol. 134, pp. 165–172, 2015.

[34] D. A. Safin and Y. Garcia, "First evidence of thermo- and two-step photochromism of tris-anils," *RSC Advances*, vol. 3, no. 18, pp. 6466–6471, 2013.

[35] B. S. Furniss, A. J. Hannaford, P. W. G. Simth, and A. R. Tatchell, *Vogel's Text Book of Practical Organic Chemistry*, Prentice Hall, 5th edition, 2008.

[21] F. L. Weitl and K. N. Raymond, "Ferric ion sequestering agents. 1. Hexadentate O-bonding N,N',N"-tris(2,3-dihydroxybenzoyl) derivatives of 1,5,9-triazacyclotridecane and 1,3,5-triaminomethylbenzene," *Journal of the American Chemical Society*, vol. 101, no. 10, pp. 2728–2731, 1979.

[22] F. L. Weitl and K. N. Raymond, "Specific sequestering agents for the actinides. 3. Polycatecholate ligands derived from 2,3-dihydroxy-5-sulfobenzoyl conjugates of diaza- and tetraazaalkanes," *Journal of the American Chemical Society*, vol. 102, no. 7, pp. 2289–2293, 1980.

[23] K. N. Raymond, G. Muller, and B. F. Matzanke, *Topics in Current Chemistry*, Springer, Berlin, Germany, 1984.

[24] G. Crisponi and M. Remelli, "Iron chelating agents for the treatment of iron overload," *Coordination Chemistry Reviews*, vol. 252, no. 10-11, pp. 1225–1240, 2008.

[25] K. N. Raymond, G. Mueller, and B. F. Matzanke, "Complexation of iron by siderophores: a review of their solution and structural chemistry and biological function," in *Topics in Current Chemistry*, F. L. Boschke, Ed., vol. 123, pp. 49–102, Springer, Berlin, Germany, 1984.

[26] M. Hayashi, K. Hirtani, M. Ishii, K. Saigo, and S. H. Kina, "Synthesis of cyclopentane-containing marine eicosanoid bacillariolide II," *Tetrahedron Letters*, vol. 39, no. 7, pp. 621–624, 1998.

[27] N. Cheraïti, M. E. Brik, G. Kunesch, and A. Gaudemer, "Synthesis of the smallest tris-(catecholamide) siderophore analogue," *Journal of Organometallic Chemistry*, vol. 575, no. 1, pp. 149–152, 1999.

[28] V. L. Pecoraro, F. L. Weit, and K. N. Raymond, "Ferric ion-specific sequestering agents. 7. Synthesis, iron-exchange kinetics, and stability constants of N-substituted, sulfonated catechoylamide analogs of enterobactin," *Journal of the American Chemical Society*, vol. 103, no. 17, pp. 5133–5140, 1981.

[29] J. C. Ryu, H. N. Shin, D. N. Kim, and S. H. Lee, "Enterobactin analogues prepared by cross-linking catechol derivative with cis,cis-1,3,5-Tris(aminomethyl)cyclohexane," *Bulletin of the Korean Chemical Society*, vol. 22, no. 12, pp. 1293–1294, 2001.

[30] B. K. Kanungo, M. Baral, S. K. Sahoo, and S. E. Muthu, "Synthesis, spectroscopic and theoretical studies of two novel tripodal imine-phenol ligands and their complexation with

[36] P. Gans, A. Sabatini, and A. Vacca, "Investigation of equilibria in solution. Determination of equilibrium constants with the HYPERQUAD suite of programs," *Talanta*, vol. 43, no. 10, pp. 1739–1753, 1996.

[37] L. Alderighia, P. Gans, A. Ienco, D. Peters, A. Sabatini, and A. Vacca, "Hyperquad simulation and speciation (HySS): a utility program for the investigation of equilibria involving soluble and partially soluble species," *Coordination Chemistry Reviews*, vol. 184, no. 1, pp. 311–318, 1999.

[38] P. Gans, A. Sabatini, and A. Vacca, "Determination of equilibrium constants from spectrophotometric data obtained from solution of known pH: the program pHab," *Annali di Chimica*, vol. 89, pp. 45–49, 1999.

[39] S. Lee, B. A. Rao, and Y.-A. Son, "A highly selective fluorescent chemosensor for Hg^{2+} based on a squaraine–bis(rhodamine-B) derivative: part II," *Sensors and Actuators B: Chemical*, vol. 210, pp. 519–532, 2015.

[40] *HyperChem Version 7.5*, Hypercube Inc, Waterloo, Canada, 2003.

[41] P. J. J. Stewart, *MOPAC2012, Version 12.239W*, Stewart Computational Chemistry, Colorado Springs, Colo, USA, 2012.

[42] S. Chaves, A. C. Mendonça, S. M. Marques et al., "A gallium complex with a new tripodal tris-hydroxypyridinone for potential nuclear diagnostic imaging: solution and *in vivo* studies of ^{67}Ga-labeled species," *Journal of Inorganic Biochemistry*, vol. 105, no. 1, pp. 31–38, 2011.

[43] A. Golcu, M. Tumer, H. Demirelli, and R. A. Wheatley, "Cd(II) and Cu(II) complexes of polydentate Schiff base ligands: synthesis, characterization, properties and biological activity," *Inorganica Chimica Acta*, vol. 358, no. 6, pp. 1785–1797, 2005.

[44] S. K. Sahoo, S. E. Muthu, M. Baral, and B. K. Kanungo, "Potentiometric and spectrophotometric study of a new dipodal ligand N,N′-bis2-[(2-hydroxybenzylidine)amino]ethylmalonamide with Co(II), Ni(II), Cu(II) and Zn(II)," *Spectrochimica Acta—Part A: Molecular and Biomolecular Spectroscopy*, vol. 63, no. 3, pp. 574–586, 2006.

[45] A. C. Mendonça, A. F. Martins, A. Melchior et al., "New tris-3,4-HOPO lanthanide complexes as potential imaging probes: complex stability and magnetic properties," *Dalton Transactions*, vol. 42, no. 17, pp. 6046–6057, 2013.

[46] N. Singh, N. Kaur, and J. F. Callan, "Incorporation of siderophore binding sites in a dipodal fluorescent sensor for Fe(III)," *Journal of Fluorescence*, vol. 19, no. 4, pp. 649–654, 2009.

[47] J. Li, N. Zhang, F. Dai, Q. Luo, and Y. Ji, "Metrological array of cyber-physical systems. Part 1. Challenge of modernity," *Sensors and Transducers*, vol. 186, pp. 125–128, 2015.

ISSN 2356-7171

Synthesis, X-Ray Crystal Structure Study, Hirshfeld Surface Analysis, and Biological Activity of N-(2-amino-phenyl)-2-methyl-benzamide

Latha Rani Nagaraju,1 Lakshmi Ranganatha Venkataravanappa,2 Sridhar MandayamAnandalwar,1 andShaukathAraKhanum3

1Department of Studies in Physics, University of Mysore, Manasagangotri, Mysuru 570 006, India 2Department of Chemistry, The National Institute of Engineering (Autonomous), Manandavadi Road, Mysuru 570 008, India 3Department of Chemistry, Yuvaraja's College, University of Mysore, Mysuru 570 005, India

1. Introduction

The title compound is a benzamide derivative. The compound consists of an amide group bridged to a benzene ring to which a methyl is attached on one side and a phenyl ring to which an amino group is attached on the other side. Benzamides are derived from benzoic acid, which are slightly soluble in water and soluble in many organic compounds.

Amides are pervasive in nature. Compounds containing amide groups show many biological activities, mainly antiproliferative, antiviral, antimalarial, general anesthetics, anti-inflammatory, and antimicrobial activities [1]. Literature reveals that the N-substituted benzamides have many pharmacologically important properties such as antifungal, antiallergic, antihypertensive, anti-inflammatory, antibacterial, analgesic, antirheumatic, antipyretic, and anti-HIV activities [2].

Hence, herein we report the synthesis, characterization, X-ray crystal structure study, *in vitro* antibacterial activity, and Hirshfeld surface analysis of N-(2-amino-phenyl)-2-methyl-benzamide.

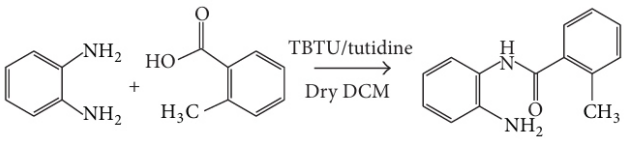

Scheme 1: Schematic diagram of the title compound.

2. Experimental

2.1. Materials and Methods. Chemicals were purchased from Sigma Aldrich Chemical Corporation. ^{1}H NMR spectra were recorded on a Bruker 400 MHz NMR spectrophotometer in DMSO-d_6 solvent and the chemical shifts were recorded in δ (ppm) downfield from tetramethylsilane. Elemental analysis was done using Perkin Elmer 2400 elemental analyzer and results are within 0.4% of the calculated value. Infrared spectra were recorded on a Perkin Elmer spectrophotometer in the range of 400–4000 cm^{-1}.

2.2. Synthesis of N-(2-amino-phenyl)-2-methyl-benzamide. The mixture of *o*-phenylenediamine (0.0037 mol) in dry dichloromethane (15 mL), 2,6-dimethyl pyridine, and 2-methyl-benzoic acid (0.0037 mol) was stirred for 30 minutes at 25–30°C. 2-(1H-Benzotriazole-1-yl)-1,1,3,3-tetramethyluronium tetrafluoroborate (0.0037 mol) was added to the mixture, whose temperature was maintained below 5°C. The reaction was monitored by Thin Layer Chromatography using chloroform : methanol (9 : 1). The reaction mass was diluted with 20 mL of dichloromethane. The organic layer was washed with water (25 mL), dried over anhydrous sodium sulfate, concentrated to syrupy liquid, and recrystallized twice by ethyl ether to afford N-(2-amino-phenyl)-2-methyl-benzamide, in good yield of 90%. The melting point of the compound is 94–96°C. The obtained crystals were white in color (Scheme 1).

Table 1: Elemental analysis for the title compound.

Element	Experimental (%)	Calculated (%)
Carbon	74.31	74.33
Hydrogen	6.24	6.25
Nitrogen	12.38	12.41

concentration reaches 0.39 × 10^{-2} mg/mL. Finally, 10 μL of bacterial suspension was added to all the wells.

The concentrations of the prepared solutions were as follows: 0.5 mg/mL, 0.25 mg/mL, 0.125 mg/mL, 0.625 × 10^{-1} mg/mL, 0.3125 × 10^{-1} mg/mL, 0.156 × 10^{-1} mg/mL, 0.78 × 10^{-2} mg/mL, and 0.39 × 10^{-2} mg/mL. Blue color indicates that the compound inhibits the growth of the bacteria, whereas pink color indicates the bacterial growth.

Inoculated plates were incubated at 37°C for 24 hours. One hour before the end of incubation 10 μL of resazurin was added to all the wells. The plates were incubated for another hour. The change in color was assessed visually. The MIC was recorded.

2.3. X-Ray Diffraction. A suitable white single crystal was selected to collect X-ray diffraction data. Data were collected on a Bruker Kappa Apex II single crystal X-ray diffractometer equipped with Cu K_α radiation and CCD detector [3]. Crystal structure was solved by direct methods using *SHELXS-97*. After locating all nonhydrogen atoms, the structure was refined by full-matrix least-squares method using *SHELXL-97* [4]. The obtained model was refined by isotropic thermal parameters later by anisotropic thermal parameter. Hydrogens were placed at chemically acceptable positions. 156 parameters were refined with 1929 unique reflections which converged the residual (R) to 0.057.

2.4. In Vitro Antibacterial Activity. As N-substituted benzamides and their derivatives have numerous biological activities, it is worthwhile to investigate the antibacterial activity of the newly synthesized compound.

Antibacterial activity was examined against two gram-positive bacteria, namely, *Bacillus subtilis* (MTCC number 121) and *Staphylococcus aureus* (MTCC number 7443), and two gram-negative bacteria, namely, *Proteus vulgaris* (MTCC number 742) and *Escherichia coli* (MTCC number 730). The bacterial strains were inoculated in nutrient broth and kept for overnight culture at 37°C. Minimum inhibitory concentration (mic) is the lowest concentration at which blue color of the dye (indicator) turns to pink color [5]. MIC was determined by microbroth dilution method using resazurin (7-hydroxy-3H-phenoxazin-3-one 10-oxide) as an indicator. Resazurin is a blue nonfluorescent, nontoxic, oxidation-reduction indicator. This was performed on 96-well microtiter plates [6].

For susceptibility testing the plates were prepared in duplicates. Nutrient broth of 50 μL was distributed to all the wells. 50 μL compound was added to third and fourth wells. Serial dilution was performed from the fourth well till the

3. Results and Discussions

3.1. Elemental Analysis. In order to confirm the chemical composition of the synthesized compound, carbon (C) and hydrogen (H) analysis was carried out. The experimental and calculated percentages of C and H are given in Table 1. The differences between experimental and calculated percentages of C and H were very small and are within the experimental errors. This confirms the formation of the product in the stoichiometric proportion.

3.2. FT-IR Spectral Analysis. In FT-IR spectra the peaks observed at 1660 cm^{-1} are assigned to C=O of carbonyl of the amide group. The peak at 1715 cm^{-1} is for N–H stretching vibrations.

3.3. ^{1}H NMR Spectral Analysis. The ^{1}H NMR spectra of the compound are shown in Figure 1. The NMR peak at δ 2.25 (s, 3H) clearly indicates that the three hydrogens of methyl group are attached to aromatic ring. The peak at δ 4.25 (bs, 2H) corresponds to the two hydrogens of the amino group. The peaks at δ 7.15–7.52 refer to eight aromatic hydrogens of the compound.

3.4. X-Ray Crystal Structure Determination. The compound $C_{14}H_{14}N_2O$ crystallizes in monoclinic crystal system, with space group $P2_1/c$. The unit cell parameters are a = 11.471(4) Å, b = 8.269(3) Å, c = 12.518(4) Å, and β = 96.155(14)°. The details of the crystal data and structure refinement are given in Table 2. The geometrical calculations were carried out using the program *PLATON* [7]. The molecular and packing diagrams were generated using *Mercury* [8]. Figure 2 shows the *ORTEP* diagram of the molecule with thermal ellipsoids drawn at 50% probability. The bond

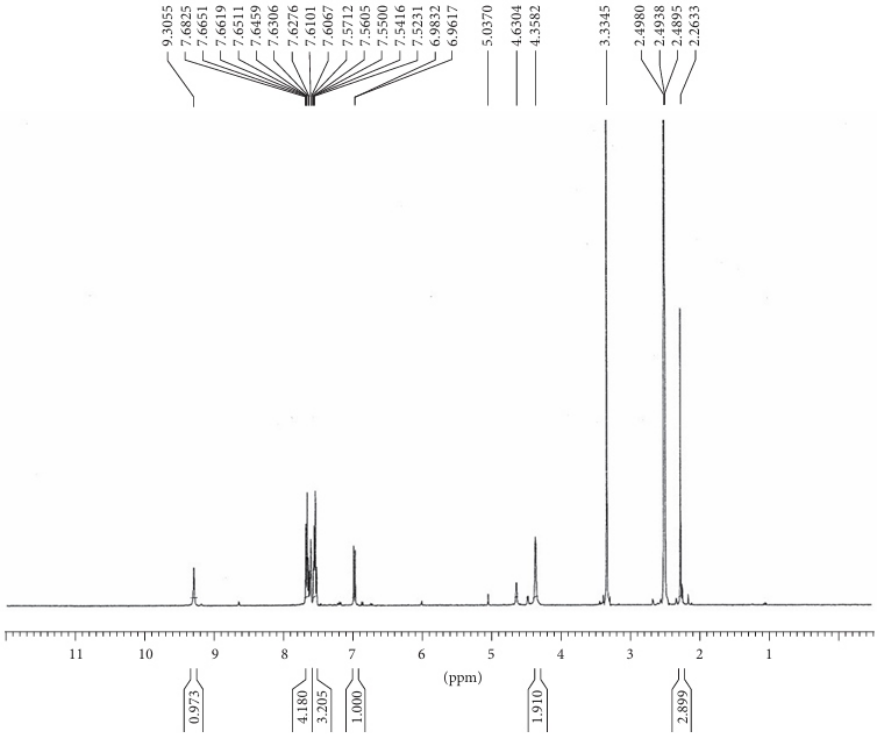

Figure 1: ^{1}H NMR spectra of the title compound.

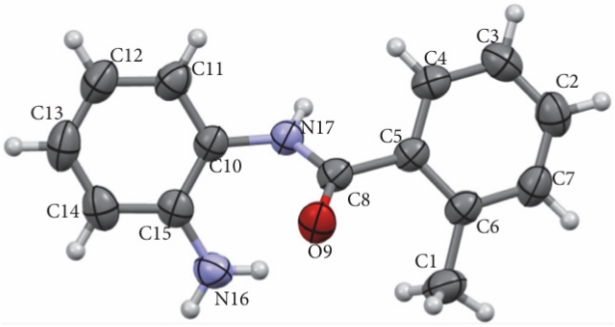

FIGURE 2: *ORTEP* diagram of the molecule with thermal ellipsoids drawn at 50% probability.

distances and angles are listed in Table 3. Torsion angles are listed in Table 4.

The phenyl rings are planar. The r.m.s. deviation of the ring C2–C7 (ring-1/*Cg*(1)) from the mean plane is 0.011(2) Å. Atoms C5 and C6 deviate by 0.010(2) Å from the mean plane defined for the ring. The r.m.s. deviation of the ring C10–C15 (ring-2/*Cg*(2)) from the mean plane is 0.000(2) Å. This ring is highly planar. The O9=C8 is 1.240(2)˚; this confirms the double bond character.

Ring-1 and ring-2 are *sp*2 hybridized. They are described by the torsion angles 1.13˚ and 0.00˚, respectively, which suggest that they adopt *+syn-periplanar (+sp)* conformation.

TABLE 2: The crystal data and structure refinement details.

CCDC deposit number	1418787
Empirical formula	$C_{14}H_{14}N_2O$
Formula weight	226.27
Temperature	293 K
Wavelength	1.54178 Å
Crystal system	Monoclinic
Space group	$P2_1/c$
Cell dimensions	a = 11.471(4) Å b = 8.269(3) Å c = 12.518(4) Å β = 96.155(14)˚
Volume	1180.5(7) Å^3
Z	4
Density (calculated)	1.273 Mg m^{-3}
Absorption coefficient	0.619 mm^{-1}
F_{000}	480
Crystal size	0.210 × 0.210 × 0.210 mm
θ range for data collection	3.88˚ to 64.69˚
Index ranges	$-13 \le h \le 13$ $-9 \le k \le 9$ $-12 \le l \le 14$
Reflections collected	9047
Independent reflections	1929 [R_{int} = 0.0384]
Refinement method	Full-matrix least-squares on F^2
Data/restraints/parameters	1929/0/156
Goodness-of-fit on F^2	1.067
Final [$I > 2\sigma(I)$]	$R1$ = 0.057, $wR2$ = 0.1627
Largest diff. peak and hole	0.267 and −0.428 eÅ^{-3}

TABLE 4: Selected torsion angles (deg.).

Atoms	Angle	Atoms	Angle
C5–C8–N17–C10	−175.47(16)	C2–C3–C4–C5	−0.6(3)
N17–C10–C11–C12	175.43(18)	C11–C10–N17–C8	124.64(19)
N17–C10–C15–C14	−175.19(16)	C4–C5–C8–N17	47.3(2)
O9–C8–N17–C10	3.7(3)	C11–C10–C15–N16	174.99(17)
C7–C2–C3–C4	1.5(3)	C11–C12–C13–C14	0.0(4)
C3–C4–C5–C6	−1.1(3)	N17–C10–C15–N16	−0.2(3)
C4–C5–C8–O9	−131.88(19)	C1–C6–C7–C2	176.30(19)

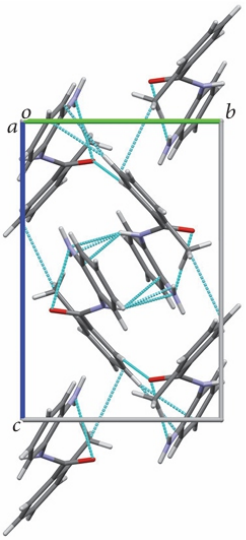

FIGURE 3: Packing of molecules when viewed along *a*-axis.

Table 3: Selected bond lengths and bond angles (Å, deg.).

Atoms	Distances	Atoms	Angles
O9–C8	1.240(2)	C8–N17–C10	125.86(14)
C1–C6	1.504(3)	N17–C10–C15	121.87(15)
N17–C8	1.346(2)	C11–C12–C13	119.14(19)
N17–C10	1.424(2)	N16–C15–C10	121.05(16)
C2–C3	1.370(3)	N16–C15–C14	120.69(17)
C14–C15	1.392(3)	C12–C13–C1	120.94(18)
C13–C14	1.375(3)	C10–C15–C14	118.06(16)
C11–C12	1.378(3)	O9–C8–N17	122.60(15)
C10–C11	1.383(3)	N17–C10–C11	117.23(16)
C12–C13	1.385(3)	C4–C5–C8	119.82(15)

Ring-1 and C=O of the amide group are *-anti-clinal (-ac),* this is confirmed by the torsion angle −131.88(19)° for C4–C5–C8–O9.

The torsion angle between two phenyl rings bridged *via* amide group is −175.47(16)° (C5–C8–N17–C10); this is greater when compared to the corresponding values of −168.48(17)° and −173.38(16)° for the isomeric benzamides 2-iodo-N-(2-nitrophenyl)benzamide (I) and N-(2-iodophenyl)-2-nitrobenzamide (II), respectively [9]. This may be due to the presence of methyl group attached to benzamide or the amino group attached to the phenyl ring or ring-2.

The packing views of the molecules down *a*- and *b*-axes are shown in Figures 3 and 4, respectively. The molecules are linked by the intermolecular interactions by three hydrogen bonds of types N–H···N, C–H···O, and C–H···π. The molecule is also stabilized by weak intermolecular interactions of type C–H···π. Atom C3 of ring-1 in a molecule acts as a donor to the C13–C14 (ring-2) atoms of another molecule. In addition, the molecule exhibits intramolecular interactions of types N–H···O and N–H···N. The hydrogen bond geometries are shown in Table 5.

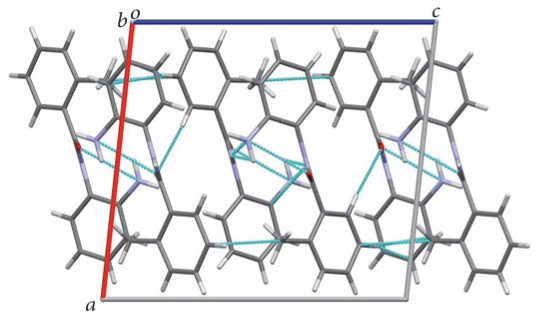

Figure 4: Packing of molecules when viewed along *b*-axis.

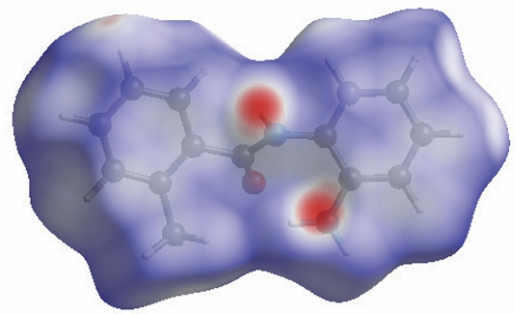

Figure 5: d_{norm} mapped on Hirshfeld surface for the visualization of the intercontacts of the title compound.

3.5. Hirshfeld Surface Analysis. *CrystalExplorer 3.1* [10] program was used for understanding the interactions and the connectivity among the molecules efficiently. The crystallographic information file (.cif) was imported to the *CrystalExplorer* to generate the Hirshfeld surfaces. The Hirshfeld surface is the region around the molecule in the crystal space which can be considered as the boundary separating two regions—the interior (the reference molecule) and the exterior (neighboring molecules) [11]. The Hirshfeld surface of the title compound is shown in Figure 5. The red region indicates the hydrogen bond acceptors of N–H···N and C–H···O interactions (N17–H17···N16 and C4–H4···O9).

The fingerprint plot shows the percentage contributions to the total Hirshfeld surface area. The fingerprint plot data is shown in Table 6. Figures 6(a), 6(b), 6(c), 6(d), 6(e), and 6(f)

Table 5: Hydrogen bond geometry (Å, deg.).

D–H···A	D–H	H···A	D···A	D–H···A
N(17)–H(17)···N(16)$^{(a)}$	0.86	2.31	3.123(2)	158
C(4)–H(4)···O(9)$^{(b)}$	0.93	2.53	3.462(3)	175
N(16)–H(16B)···O(9)*	0.86	2.47	2.948(2)	116
N(16)–H(16B)···N(17)*	0.86	2.57	2.874(2)	102

*Intramolecular hydrogen bond interactions.
Symmetry codes: (a) $1-x, 1-y, 1-z$; (b) $1-x, 1/2+y, 3/2-z$.

Table 6: Percentage of various intermolecular contacts contributing to Hirshfeld surface.

Intercontacts	Contribution (%)	Intercontacts	Contribution (%)
H···H	56.0	C–C	3.4
C–H/H···C	27.7	N–H/H···N	2.6
O–H/H···O	9.8	N–O/O–N	0.4

Table 7: MIC of the title compound against various bacterial strains.

Bacterial strains	MIC (mg/mL)	
	Streptomycin (std.)	Compound
Bacillus subtilis	$0.3125 \cdot 10^{-1}$	0.125
Staphylococcus aureus	$0.3125 \cdot 10^{-1}$	0.125
Proteus vulgaris	$0.156 \cdot 10^{-1}$	$0.625 \cdot 10^{-1}$
Escherichia coli	$0.78 \cdot 10^{-2}$	0.25

and NMR confirms the chemical compositions of the compound. The structure was confirmed by the single crystal X-ray diffraction. The intermolecular interactions were studied by Hirshfeld surface analysis. Screening for biological activity showed that the compound shows better antibacterial activity against gram-negative bacteria *Proteus vulgaris.*

show the fingerprint plots of the title compound. The major contribution (56.0%) is from H···H contacts. In Figure 6(a) the wings are due to the C–H···π interactions.

3.6. In Vitro Antimicrobial Activity. The results of biological activity of the title compound are given in Table 7. The resazurin assay showed that the compound has lower-to-average activity against various tested bacterial strains. The results of the compound with tested bacterial strains were compared with streptomycin. Streptomycin was used as standard in the experiment. The compound showed better/average activity against gram-negative bacteria *Proteus vulgaris* than any other bacteria, though it never outperforms streptomycin.

4. Conclusion

In this research work we have discussed the synthesis of the compound N-(2-amino-phenyl)-2-methyl-benzamide. The preliminary characterizations like elemental analysis, FT-IR,

Competing Interests

The authors declare that there is no conflict of interests regarding the publication of this paper.

Acknowledgments

The authors are thankful to IoE, Vijnana Bhavana, University of Mysore, Mysuru, for collecting XRD data, to Dr. Maheshwar P. K. and Mr. Nandu, Department of Microbiology, Yuvaraja's College (Autonomous), University of Mysore, Mysuru, for the assistance in evaluating the biological activity. Latha Rani Nagaraju is thankful to UGC, New Delhi, for RFSMS fellowship. Shaukath Ara Khanum acknowledges the financial support provided by the Vision Group on Science and Technology, Government of Karnataka, under the scheme CISEE (VGST/CISSE/2012-13/2882), Department of Information Technology, Biotechnology and Science & Technology, Bengaluru.

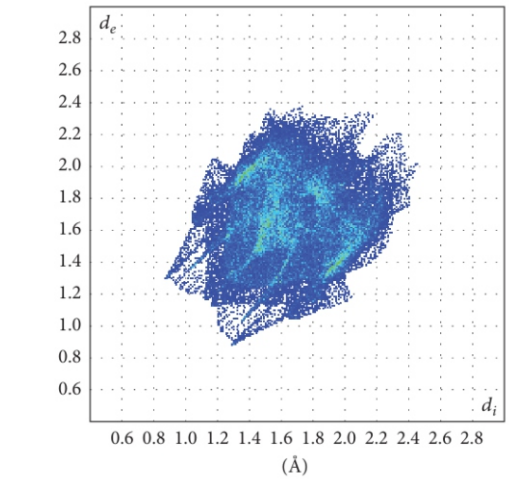

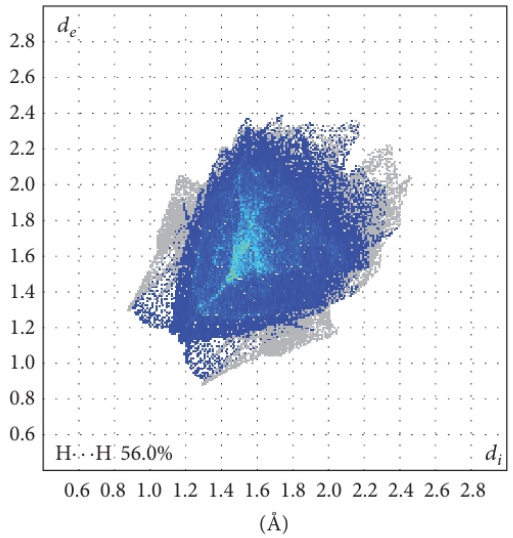

(b)

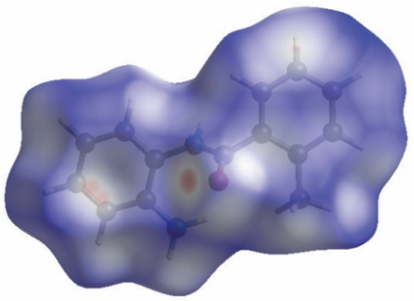

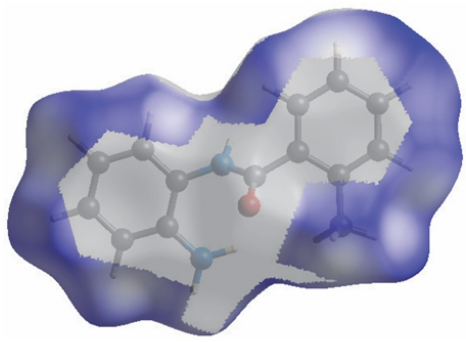

(e)

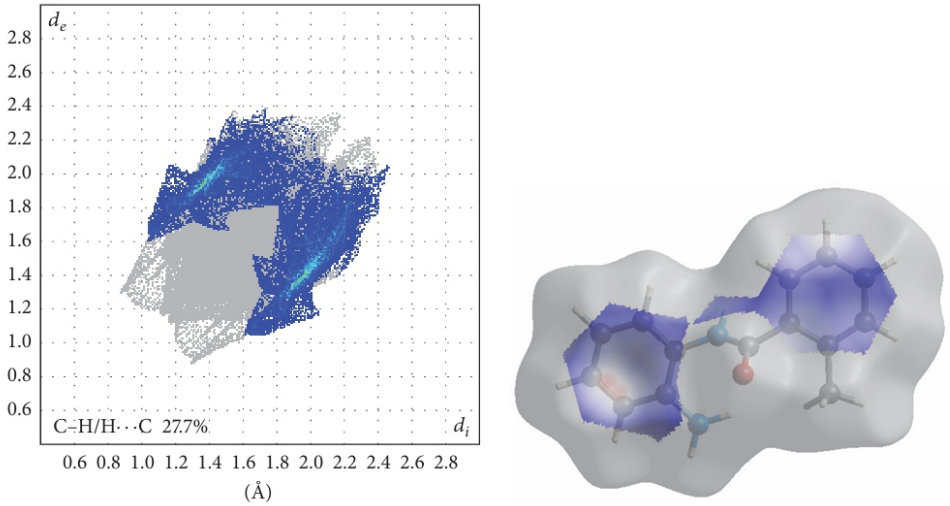

FIGURE 6: Fingerprint plot of the title compound. (a) Highlighting full two-dimensional map. (b) Two-dimensional map resolved into H···H contacts. (c) Two-dimensional map resolved into C–H/H···C contacts. (d) All contacts. (e) Major H···H contacts. (f) Major C–H contacts.

References

[1] B. S. Priya, S. Naveen, G. Sarala et al., "Crystal structure of 2-ethoxy-*N*-[4-(pyrimidin-2-ylsulfamoyl)-phenyl]-benzamide," *Analytical Sciences: X-Ray Structure Analysis Online*, vol. 22, pp. x235–x236, 2006.

[2] A. Saeeda, N. A. Al-Masoudi, and C. Pannecouque, "*In-vitro* anti-HIV activity of new thiazol-2-ylidene substituted benzamide analogues ," *Der Pharma Chemica*, vol. 4, no. 1, pp. 106–115, 2012.

[3] Bruker, *APEX2, SAINT, & SADABS*, Bruker AXS Inc, Madison, Wis, USA, 2009.

[4] G. M. Sheldrick, *SHELX 97. A Program for Crystal Structure Determination*, Cambridge University Press, Cambridge, UK, 1997.

[5] S. D. Sarker, L. Nahar, and Y. Kumarasamy, "Microtitre plate-based antibacterial assay incorporating resazurin as an indicator of cell growth, and its application in the *in vitro* antibacterial screening of phytochemicals," *Methods*, vol. 42, no. 4, pp. 321–324, 2007.

[6] A. H. Deborah and J. S. Neil, "Resazurin-based assay for screening bacteria for radiation sensitivity," *Methodology*, vol. 2, no. 55, pp. 1–6, 2013.

[7] A. L. Spek, "Structure validation in chemical crystallography," *Acta Crystallographica*, vol. 65, pp. 148–155, 2009.

[8] C. F. Macrae, I. J. Bruno, J. A. Chisholm et al., "Mercury CSD 2.0—new features for the visualization and investigation of crystal structures," *Journal of Applied Crystallography*, vol. 41, no. 2, pp. 466–470, 2008.

[9] J. L. Wardell, J. M. S. Skakle, J. N. Low, and C. Glidewell, "Contrasting three-dimensional framework structures in the isomeric pair 2-iodo-*N*-(2-nitrophenyl)benzamide and *N*-(2-iodophenyl)-2-nitrobenzamide," *Acta Crystallographica Section C Crystal Structure Communications*, vol. 61, no. 11, pp. o634–o638, 2005.

[10] S. K. Wolff, D. J. Grimwood, J. J. McKinnon, D. Jayatilaka, and M. A. Spackamn, *Crystal Explorer 3.1*, University of Western Australia, Perth, Australia, 2007.

[11] J. Christian, E. Krzysztof, and H. Loic, "The enrichment ratio of atomic contacts in crystals, an indicator derived from the Hirshfeld surface analysis," *International Union of Crystallography (IUCr)*, vol. 1, part 2, pp. 119–128, 2014.

ISSN 2356-7171

Removal of Fluoride from Water by Adsorption onto Fired Clay Pots: Kinetics and Equilibrium Studies

G. P. Kofa,1,2 V. H. Gomdje,2 C. Telegang,1 and S. Ndi Koungou1

1Water Treatment and Filtration Research (Chem. Eng.) Group, Department of rocess Engineering, ENSAI, UniversityofNgaoundere,P.O.Box455,Ngaoundere,Cameroon

2Higher Institute of Sahel (ISS), University of Maroua, Maroua, Cameroon

ABSTRACT

Excessive fluoride in potable water is a serious health problem in rural areas of many developing countries. Hence, there is a need to find a simple and cost-effective method for water defluoridation in such areas. In the northern part of Cameroon, clay pots are used for cooking food and water storage. The firing of these pots consists of intensive burning using fire wood. They were tested as a potential adsorbent for removing excess fluoride from water. Experiments were carried out in a jar test at room temperature (25 ± 2 C). Effects of contact time (0–90min), pH (4, 5, 7, 8, and 9), stirring speed (60, 90, 120, and 200rpm), and ionic strength (0–1000mg/L) were investigated. Results showed that equilibrium was attained in 10min whatever the pH. Pseudo-second-order andporediffusion models described well the adsorption process. The highest amount of fluoride adsorbed (1.6mg/g) was obtained at pH 4-5 and the optimum stirring speed is 120rpm. Ionic strength has a significant effect on fluoride adsorption.

1. Introduction

Fluoride ion exists in natural waters and it is an essential micronutrient in humans in preventing dental caries and in facilitating the mineralization of hard tissues if taken at a recommended range of concentration. Higher level of fluoride in groundwater is a worldwide problem [1–3]. The World Health Organization (WHO) has set a guideline of 1.5 mg/L for fluoride in potable water [4]. Concentration higher than this value can lead to fluorosis (dental and/or skeletal) and several types of neurological damage in severe cases [5]. Many methods have been developed for fluoride removal from water such as adsorption [6], ion exchange [7], membrane processes such as reverse osmosis and nanofiltration [8, 9], electrodialysis [10, 11], and precipitation [12]. Among these methods, adsorption is a widely used method for defluoridation which depends on ions (adsorbate) in fluid diffusing to the surface of a solid (adsorbent) when they are bound to the solid surface or are held there by weak intermolecular forces [13]. Adsorption is recognized as the most efficient, promising, and widely used fundamental approach in water and wastewater treatment processes [14].

Figure 1: Firing process of clay pots.

Different adsorbents such as activated alumina [15], bleaching earth [16], iron oxide [17], activated titanium rich bauxite [18], activated carbon [19], red mud [20], and clay [21, 22] were tested to find out efficient and economically viable defluoridating ones. Among these adsorbents, clay and clay minerals are naturally abundant, renewable, and environmentally sustainable [23–25]. They are considered robust adsorbents [24] due to their low cost, sorption properties, and ion exchange potential. In recent years, considerable amount of work has been done on activation of clay and clay minerals to improve the adsorption capacity and hence removal efficiency [26, 27]. Chemical and physical activation methods are commonly used. However chemical treatment has not always proven to be effective. For example, Ma et al. [28] reported equilibrium fluoride adsorption capacity by granular acid treatment of bentonite of just 0.07 mg/g. That is why some researchers turn to heat treatment which can also increase ions adsorption capacity in clay [29, 30].

Clay pot is made of a mixture of different types of natural clays. The process consists of mixing the different clay fractions, forming the pot, and burning under an intensive wood fire (around 300°C) where they get cooked. During

Table 1: Elemental compositions of Kouladje fired clays obtained by EDAX.

Elements	Weight (%)	Atomic (%)
Oxygen (O)	40.26	55.02
Sodium (Na)	0.20	0.19
Magnesium (Mg)	0.25	0.23
Aluminium (Al)	3.48	2.82
Silicon (Si)	51.30	39.93
Potassium (K)	0.27	0.15
Iron (Fe)	4.23	1.66

the firing process (cooking phase) some of them get broken. These broken pots are not useful for water storage but could be used as an adsorbent, because they are primary heated clays. The main objective of this investigation is to study the removal efficiency of fired clay pots powder as a potential adsorbent for fluoride removal under different physicochemical conditions.

2. Materials and Methods

2.1. Materials. Clay pots were collected from Kouladje, a village in the northern part of Cameroon. The firing of these pots consists of its intensive burning using fire wood (Figure 1). The clay powder was obtained after crushing and sieving a clay pot with standardized stainless sieves and the fraction less than 100 μm was collected.

All other reagents used in the present study were of analytical grade. A stock solution of fluoride 1000 mg/L was prepared by dissolving appropriate quantity of sodium fluoride (Sigma-Aldrich, USA) in distilled water.

2.2. Characterization of Adsorbent. The surface morphology of the fired clay powder was examined using scanning electron microscopy (Hitachi S-3000H, Japan) microscope with an accelerating voltage of 15 kV. EDAX was also performed on the same device. The specimens were prepared using carbon tape.

2.3. Batch Adsorption Studies. Adsorption experiments were carried out on a jar test (batch mode) at different pH (4, 5, 7, 8, and 9) ionic strengths (0–1000 mg/L) and stirring speed (60, 90, 120, and 200 rpm). In a typical run, beakers (1 L) were filled with 500 mL of fluoride solution of predetermined concentration, with pH adjusted to the desired value with 0.1 M NaOH or 0.1 M HCl solution. The ionic strength of the solution was also adjusted by adding KNO_3 solution. A predetermined amount of adsorbent was added to the beaker and the resulting suspension was stirred at a fixed speed. After a given time, the stirring stopped, the suspension was centrifuged (BIOFUGE Heraeus, Germany) at 950g, and the supernatant was filtered on a Minisart X50 (Prolabo, France) membrane filter of porosity 0.1 μm. The residual fluoride concentration in the aqueous solution was measured by means of a multiparameter analyser (Consort 869, Belgium) equipped with fluoride ion specific electrode (ELITE 201, England).

Isotherm experiments were carried out at pH = 4, by varying fluoride concentration ranging from 1 to 64 mg/L. The amount of fluoride adsorbed (q) was calculated as the change in the aqueous phase concentration from initial value according to

$$q = \frac{(C_0 - C)}{m} \times V, \tag{1}$$

where C_0 and C (mg/L) are the initial fluoride concentration and at contact time t, (min), V (L) is the volume of solution, and m (mg) is the amount of adsorbent added.

3. Results and Discussion

3.1. Morphological and Elemental Composition of Fired Clay. Clay morphology at different magnification is presented on Figure 2. It is observed from this figure that the morphology of the fired clay is compact with interlayers which are favorable for adsorption phenomena. This compactness of the morphology is due to the effect of the temperature applied on these clays during the firing process of pots. The EDAX spectrum of Figure 3 showed the presence of Na, Mg, Al, Si, Fe, K, and O. Clay is mainly composed of silica as shown in Table 1 and can be explained by the fact that the extraction zone is composed of the sand-clay types [31].

3.2. Kinetic Study. The kinetic study was carried out in an agitated vessel as described earlier by changing the various operating conditions.

3.2.1. Effects of pH. Figure 4 shows a comparison of the amount of fluoride adsorbed at different pH as a function of contact time. The examination of these kinetic curves reveals a rapid adsorption to attain the equilibrium adsorption. In all the pH used, two phases were observed: (a) the first phase, where the adsorption is rapid and appeared within the 10 min contact time; (b) the second phase, where the amount of fluoride adsorbed remained constant after 10 min of contact time, implying that equilibrium was reached. In general, the fast adsorption could be attributed to a surface reaction process. It is also shown in Figure 4 that the adsorption density decreases with the increase of pH. This can be

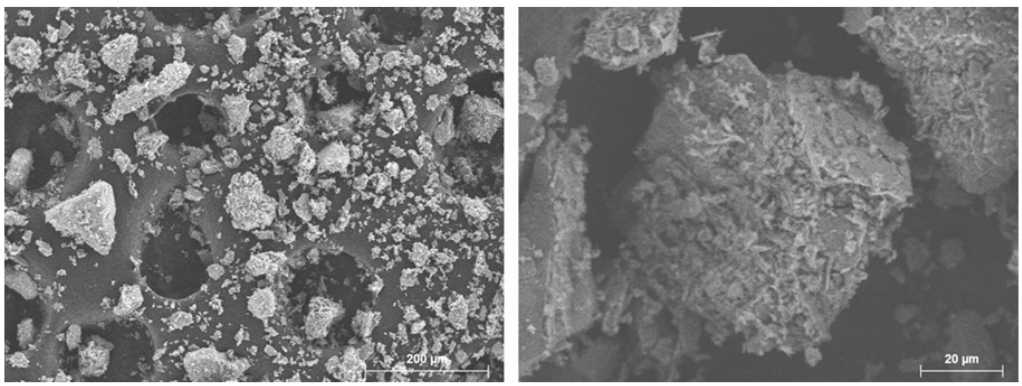

Figure 2: Electron microscopy image of clay pot powder at different magnification.

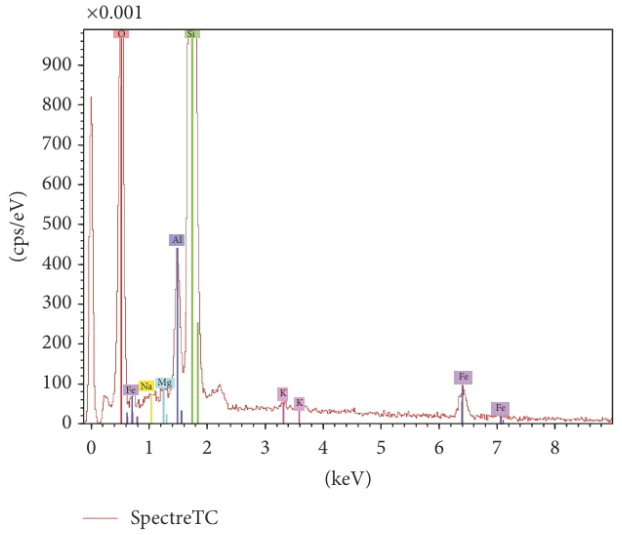

Figure 3: EDAX spectrum of the fired clay pots.

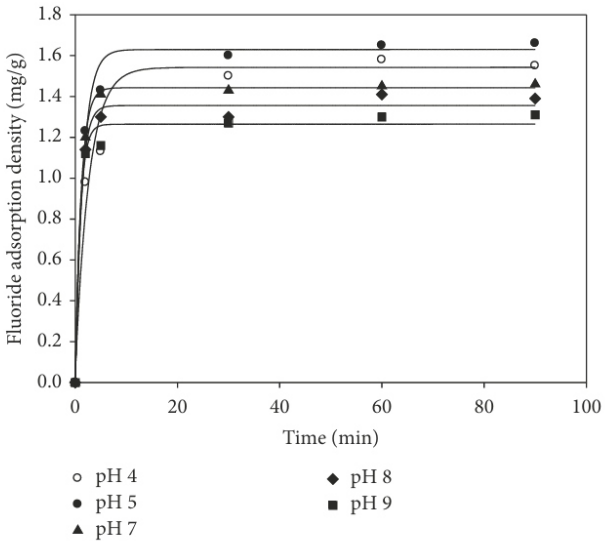

Figure 4: Adsorption kinetics at different pH (stirring speed 120 rpm; initial fluoride concentration = 10 mg/L; adsorbent dose = 1 g/L, $T = 25 \pm 2^{\circ}C$).

attributed to competition between hydroxide and fluoride ion having the same charge and similar radius [32]. The maximum adsorption was obtained at the pH 5. The obtained result for maximum adsorption is in agreement with fluoride removal studies on red mud (pH 5.5) [20], refractory grade bauxite (pH 5.5) [33]. Adsorption is also not favored in the acid range; this may be a result of the formation of weakly ionized hydrofluoric acid [20].

The pseudo-first-order, pseudo-second-order, and intraparticle diffusion models were used to test the adsorption kinetics data to investigate the mechanism of adsorption. The pseudo-first-order rate expression of Lagergren is given as [34]

$$\log(q_e - q_t) = \log q_e - \frac{k_1}{2{,}303}t, \tag{2}$$

where q_t (mg/g) is the amount of adsorbed fluoride at time t, k_1 (min^{-1}) is the rate constant of the first-order reaction, and q_e is the equilibrium sorption uptake derived from extrapolation of experimental data at time t = infinity. A straight line of $\log(q_e - q_t)$ versus t suggests the applicability of this kinetic model (Figure 5(a)). q_e and k_1 (Table 2) were determined from the intercept and slope of the plot, respectively.

The pseudo-second-order kinetic model [34] is integrated and linearized form has been used:

$$\frac{t}{q_t} = \frac{1}{k_2 q_e^2} + \frac{1}{q_e}t. \tag{3}$$

The plot of t/q_t versus t (Figure 5(b)) gave a straight line showing that second-order kinetic model was applicable and q_t and k_2 (Table 2) were determined from the slope and intercept of the plot, respectively.

From Table 2, the values of correlation coefficients obtained for the pseudo-first-order reaction were not appropriate to describe the adsorption of fluoride on fired clay. On the contrary, the values of correlation coefficients for pseudo-second-order model were all greater than 0.95 and the adsorption capacities calculated by the model are close to those determined by experiments. Hence, the data was well correlated by the pseudo-second-order model as shown in Figure 5. This fact suggested that the rate of fluoride

Table 2: Kinetics parameters for adsorption of fluoride on fired clay.

Initial concentration (mg/L)	First-order model				Second-order model			Intraparticle diffusion model	
	$q_{e,\text{exp}}$ (mg/g)	k_1 (min^{-1})	$q_{e,\text{cal}}$ (mg/g)	R^2	k_2 ($\text{g·mg}^{-1}\text{min}^{-1}$)	$q_{e,\text{cal}}$ (mg/g)	R^2	k_p ($\text{mg·g}^{-1}\text{·min}^{-0.5}$)	R^2
10	1.40	0.25	0.87	0.87	0.48	1.30	0.97	0.45	0.99
40	2.17	0.49	0.90	0.90	0.28	2.06	0.98	0.73	0.98

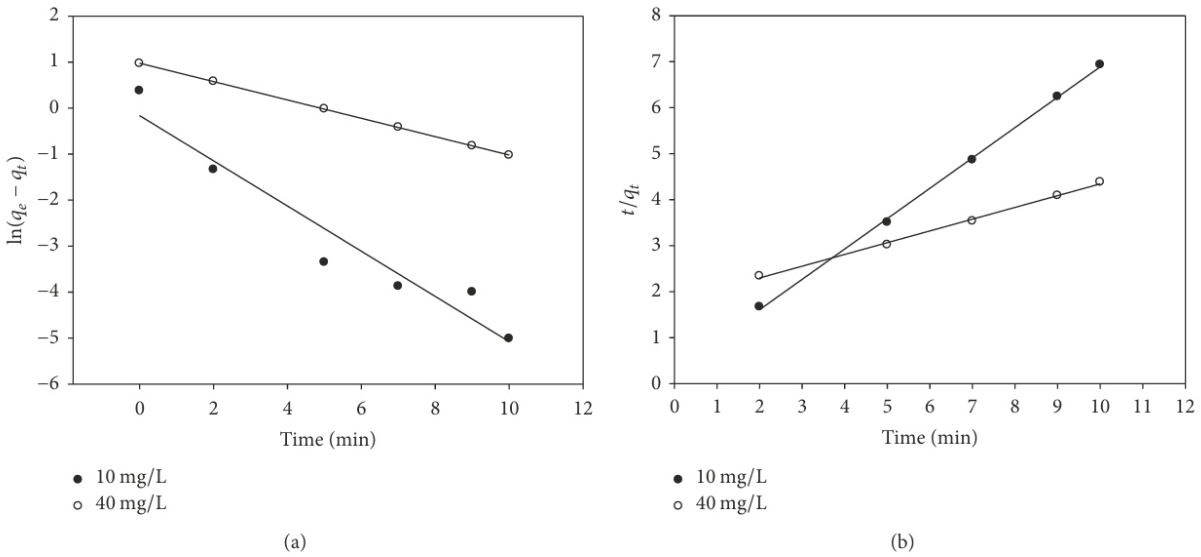

Figure 5: First-order (a) and second-order kinetics modeling of fluoride adsorption on fired clay pots (adsorbent dose 1 g/L, pH = 7, and temperature 25 ± 2°C).

adsorption onto fired clay is dependent on the availability of adsorption sites rather than the adsorbate concentration in solution [35].

To evaluate the limiting rate of the fluoride adsorption on fired clay, the possible contribution of intraparticle diffusion on fluoride adsorption process was explored using Weber-Morris model [36]:

$$q = k_{\text{int}} t^{0,5} + C, \tag{4}$$

where k_{int} can be calculated from the slope of the plot of q versus $t^{1/2}$. As shown in Figure 6(a), the linear portion of plot is not passing through the origin at each of the tested concentrations, which indicates the fluoride adsorption on fired clay is a complex procedure. Both the surface adsorption as well as intraparticle diffusion contributes to the rate determining step [16, 37].

The data was further used to investigate the slow step occurring in the present adsorption system. The applicability of Bahangam's equation [38] was tested

$$\log\log\left(\frac{C_0}{C_0 - qm}\right) = \log\left(\frac{k_0 m}{2{,}303V}\right) + \alpha \log t, \tag{5}$$

where C_0 is the initial concentration of the adsorbate in solution (mg/L), V is the volume of the solution (L), m is the weight of adsorbent used per liter of solution, q is the amount of adsorbate retained at time t, and α (<1) and k_0 are constants to the present system which was examined. As such, $\log\log(C_0/(C_0 - qm))$ was plotted against $\log t$ in Figure 6(b). The plot was found to be linear and the correlation coefficients are greater than 0.95 indicating that kinetics confirms Bahangam's equation and therefore the adsorption of fluoride on fired clay was pore diffusion controlled [37].

3.3. Adsorption Isotherms. Fluoride ion adsorption was carried out at pH 4 and stirring speed of 120 rpm. Two isotherms equations have been applied for this study, Langmuir and Freundlich. The linear form of the Langmuir equation is given by

$$\frac{C_e}{q_e} = \frac{C_e}{Q_m} + \frac{1}{Q_m b}, \tag{6}$$

where q_e and C_e are the equilibrium concentrations of fluoride in the adsorbed (mg/g) and liquid phases (mg/L), respectively. Q_m and b are the Langmuir constants which are related to the adsorption capacity and energy of adsorption, respectively, and can be calculated from the intercept and slope of the linear plot, with C_e/q_e versus C_e.

The adsorption equilibrium data was also applied to Freundlich isotherm model. The linear form of the model can be expressed as follows:

$$\log q_e = \log k_F + \frac{1}{n} \log C_e, \tag{7}$$

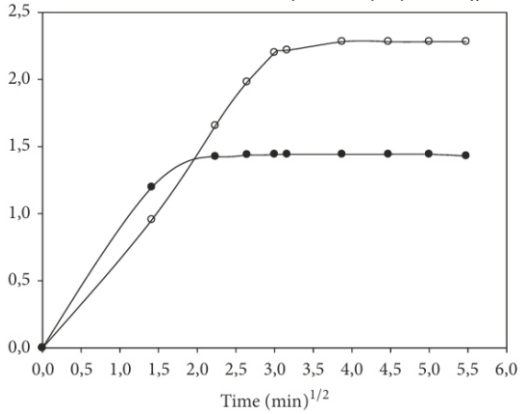

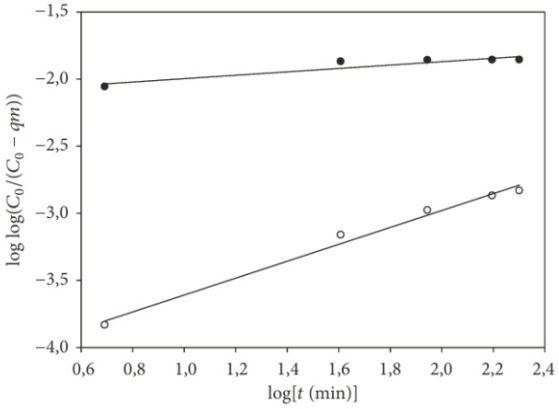

(a) (b)

Figure 6: Intraparticle diffusion model (a) and Bahangam's equation plot (b) (adsorbent dose 1 g/L, pH = 7, and temperature 25 ± 2°C).

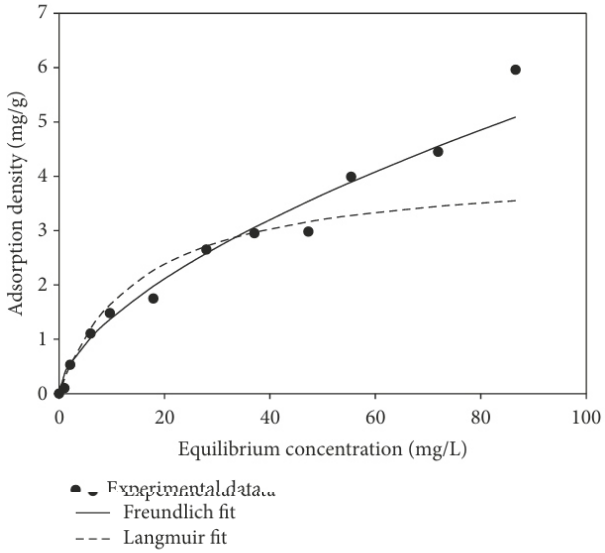

Figure 7: Adsorption isotherms of fluoride on fired clay pots (stirring speed 120 rpm; pH = 4; contact time = 30 min).

where q_e and C_e are the equilibrium concentration of fluoride in the adsorbed (mg/g) and liquid phases (mg/L), respectively. k_F and n are the Freundlich constants which are related to adsorption capacity and intensity, respectively. These constants can be calculated from the slope and intercept of the linear plot, with $\log q_e$ versus $\log C_e$.

To show the ability of different isotherms to correlate with experimental results, the theoretical plots from each isotherm have been fitted with the experimental data for adsorption of fluoride on fired clay pots (Figure 7). Langmuir and Freundlich parameters and regression coefficients (R^2) are presented in Table 3. From Figure 7, the adsorption data fitted well with Freundlich isotherm model indicating the heterogeneous distribution of active sites on fired clay pot [39]. The value of the correlation coefficient is 0.98, indicating a good mathematical fit. The Langmuir plot model has lower R^2 than the Freundlich model. In order to predict the adsorption efficiency of the adsorption process, the dimensionless equilibrium parameters were determined by using the following equation:

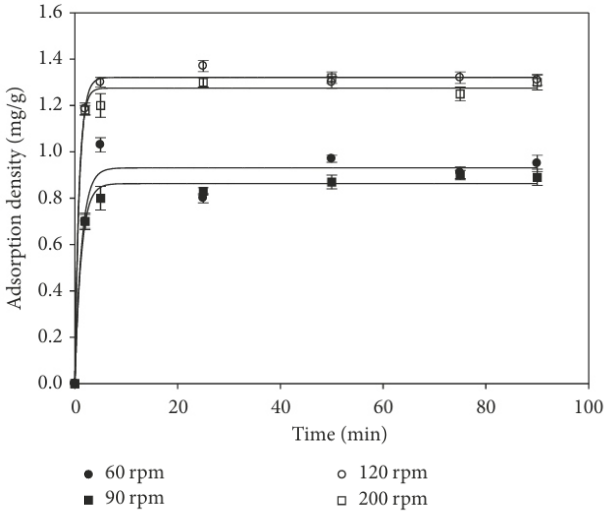

Table 3: Langmuir and Freundlich isotherms parameters for the adsorption of fluoride on fired clay pots.

Models	Parameters		
Langmuir	b (L·mg^{-1})	q_{max} (mg/g)	R^2
	0.067	4.16	0.95
Freundlich	k_f (mg/g)	n	R^2
	0.35	0.602	0.98

$$R = \frac{1}{1 + bC_0}, \tag{8}$$

where C_0 is the initial concentration and b is the Langmuir isotherm constant.

The value of R varied from 0.93 to 0.19. These values are less than 1, indicating the favorable adsorption of fluoride on fired clay [16].

3.4. Effect Stirring Speed. Effects of stirring speed on the adsorption of fluoride are presented in Figure 8. It is clear from the figure that the adsorption density increases with agitation speed up to 120 rpm and beyond this it is almost constant. The external mass transfer increases with the agitation speed, resulting in an increase in fluoride transport from the bulk to the adsorbent sites and thereby increasing the rate of adsorption. Fluoride adsorption density is almost invariant beyond 120 rpm, as the external mass transfer not affected by the variations of the ionic strength, then an inner sphere surface complexation should form, whereas the presence of outer sphere complexes is indicated by changes in adsorption with changing ionic strength. Based on this theory, it is postulated that the adsorption of fluoride on fired clay pots may take place by the formation of outer sphere complexation.

4. Conclusion

Adsorption of fluoride onto fired clay pots from Cameroon has been studied in detail. Fired clay is composed of different oxides. Kinetic studies reveal that equilibrium is attained within 10 min whatever the pH studied. The maximum adsorbed fluoride is 1.3 mg/g at a stirring speed of 120 rpm. Adsorption follows pseudo-second-order and both the surface adsorption and intraparticle diffusion contribute to the rate determining step. Freundlich isotherm fits the

Figure 8: Effect of stirring speed on adsorption density of fluoride on fired clay pot powder (pH = 4; initial fluoride concentration = 10 mg/L).

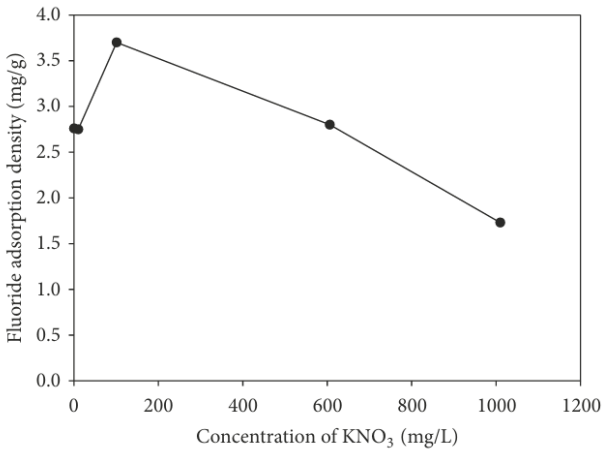

Figure 9: Effect of ionic strength (KNO_3 salt) on adsorption density of fluoride on clay pots powder (pH = 4, initial fluoride concentration = 20 mg/L, and contact time = 20 min).

resistance does not decrease appreciably beyond this rpm. Therefore, it was suggested that 120 rpm could be suitable for fluoride adsorption by fired clay and no reduction of fluoride retention was observed as found by Ndi et al. [22].

3.5. Effect of Ionic Strength. The effect of ionic strength on fluoride adsorption was studied by varying the concentration of KNO_3 (0–1000 mg/L) (Figure 9). The result showed that the amount of fluoride adsorbed on fired clay pot was significantly affected when the concentration increases from 0 to 1000 mg/L KNO_3. The same effect of ionic strength was also observed for the adsorption of Cr(VI) on bentonite [40]. Studying the influence of ionic strength is a simple approach to distinguish between inner sphere and outer sphere surface complexes when direct evidence from microscopic data is absent. According to Hayes et al. [41], if the adsorption is adsorption data adequately. The effect of ionic strength has a significant effect on fluoride adsorption.

Being a useless and abundantly available material, fired clay pots can be used for industrial application for removing fluoride from water.

Conflicts of Interest

The authors declare that they have no conflicts of interest.

References

[1] W. Y. Fantong, H. Satake, S. N. Ayonghe et al., "Geochemical provenance and spatial distribution of fluoride in groundwater of Mayo Tsanaga River Basin, Far North Region, Cameroon: implications for incidence of fluorosis and optimal consumption dose," *Environmental Geochemistry and Health*, vol. 32, no. 2, pp. 147–163, 2010.

[2] C. Neal, M. Neal, H. Davies, and J. Smith, "Fluoride in UK rivers," *Science of the Total Environment*, vol. 314-316, pp. 209–231, 2003.

[3] R. Tekle-Haimanot, Z. Melaku, H. Kloos et al., "The geographic distribution of fluoride in surface and groundwater in Ethiopia with an emphasis on the Rift Valley," *Science of the Total Environment*, vol. 367, no. 1, pp. 182–190, 2006.

[4] WHO (World Health Organization, Guidelines for Drinking Water Quality), World Health Organization, Geneva, 2006.

[5] Meenakshi and R. C. Maheshwari, "Fluoride in drinking water and its removal," *Journal of Hazardous Materials*, vol. 137, no. 1, pp. 456–463, 2006.

[6] H. Lounici, L. Addour, D. Belhocine et al., "Study of a new technique for fluoride removal from water," *Desalination*, vol. 114, no. 3, pp. 241–251, 1997.

[7] K. Vaaramaa and J. Lehto, "Removal of metals and anions from drinking water by ion exchange," *Desalination*, vol. 155, no. 2, pp. 157–170, 2003.

[8] M. S. Onyango and H. Matsuda, "Fluoride removal from water using adsorption technique," *Advances in Fluorine Science*, vol. 2, pp. 1–48, 2006.

[9] M. Tahaikt, R. El Habbani, A. Ait Haddou et al., "Fluoride removal from groundwater by nanofiltration," *Desalination*, vol. 212, no. 1-3, pp. 46–53, 2007.

[10] M. A. M. Sahli, S. Annouar, M. Tahaikt, M. Mountadar, A. Soufiane, and A. Elmidaoui, "Fluoride removal for underground brackish water by adsorption on the natural chitosan and by electrodialysis," *Desalination*, vol. 212, no. 1-3, pp. 37–45, 2007.

[11] E. Ergun, T. Ali, C. Yunus, and K. Izzet, "Electrodialytic removal of fluoride from water: Effects of process parameters and accompanying anions," *Separation and Purification Technology*, vol. 64, no. 2, pp. 147–153, 2008.

[12] E. J. Reardon and Y. Wang, "A limestone reactor for fluoride removal from wastewaters," *Environmental Science & Technology*, vol. 34, no. 15, pp. 3247–3253, 2000.

[13] T. N. De Castro Dantas, A. A. D. Neto, and M. C. P. De A. Moura, "Removal of chromium from aqueous solutions by diatomite treated with microemulsion," *Water Research*, vol. 35, no. 9, pp. 2219–2224, 2001.

[14] K. Y. Foo and B. H. Hameed, "Insights into the modeling of adsorption isotherm systems," *Chemical Engineering Journal*, vol. 156, no. 1, pp. 2–10, 2010.

[15] S. Ghorai and K. K. Pant, "Equilibrium, kinetics and breakthrough studies for adsorption of fluoride on activated alumina," *Separation and Purification Technology*, vol. 42, no. 3, pp. 265–271, 2005.

[27] A. Maiti, J. K. Basu, and S. De, "Chemical treated laterite as promising fluoride adsorbent for aqueous system and kinetic modeling," *Desalination*, vol. 265, no. 1-3, pp. 28–36, 2011.

[28] Y. Ma, F. Shi, X. Zheng, J. Ma, and C. Gao, "Removal of fluoride from aqueous solution using granular acid-treated bentonite (GHB): batch and column studies," *Journal of Hazardous Materials*, vol. 185, no. 2-3, pp. 1073–1080, 2011.

[29] J. Osei, S. K. Gawu, A. I. Schäfer, F. A. Atipoka, and F. W. Momade, "Impact of laterite characteristics on fluoride removal from water," *Journal of Chemical Technology and Biotechnology*, vol. 91, no. 4, pp. 911–920, 2016.

[30] C.-H. Weng, C.-Z. Tsai, S.-H. Chu, and Y. C. Sharma, "Adsorption characteristics of copper(II) onto spent activated clay," *Separation and Purification Technology*, vol. 54, no. 2, pp. 187–197, 2007.

[31] B. Najet, K. Lassine, K. Atsushi et al., "Electrochemical analysis of endocrine disrupting chemicals over carbon electrode modified with cameroon's clay," *Journal of the Electrochemical Society*, vol. 162, no. 1, pp. B1–B8, 2015.

[32] A. Vinati, B. Mahanty, and S. K. Behera, "Clay and clay minerals for fluoride removal from water: a state-of-the-art review," *Applied Clay Science*, vol. 114, pp. 340–348, 2015.

[16] M. Mahramanlioglu, I. Kizilcikli, and I. O. Bicer, "Adsorption of fluoride from aqueous solution by acid treated spent bleaching earth," *Journal of Fluorine Chemistry*, vol. 115, no. 1, pp. 41–47, 2002.

[17] E. Kumar, A. Bhatnagar, M. Ji et al., "Defluoridation from aqueous solutions by granular ferric hydroxide (GFH)," *Water Research*, vol. 46, pp. 1–9, 2008.

[18] D. Nigamananda, P. Pragyan, and R. Rita, "Defluoridation of drinking water using activated titanium rich bauxite," *Journal of Colloid and Interface Science*, vol. 292, no. 1, pp. 1–10, 2005.

[19] R. S. Sathish, N. S. R. Raju, G. S. Raju, G. N. Rao, K. A. Kumar, and C. Janardhana, "Equilibrium and kinetic studies for fluoride adsorption from water on zirconium impregnated coconut shell carbon," *Separation Science and Technology*, vol. 42, no. 4, pp. 769–788, 2007.

[20] Y. Çengeloğlu, E. Kir, and M. Ersöz, "Removal of fluoride from aqueous solution by using red mud," *Separation and Purification Technology*, vol. 28, no. 1, pp. 81–86, 2002.

[21] P. P. Coetzee, L. L. Coetzee, R. Puka, and S. Mubenga, "Characterisation of selected South African clays for defluoridation of natural waters," *Water SA*, vol. 29, no. 3, pp. 331–338, 2003.

[22] K. Ndi, G. Kofa, T. Metiotsop, and G. Kayem, "Removal of excess Fluoride from water using Laterite and Kaolinite," in *Proceedings of the Conférence de Société Française de Génie des Procédés*, Marseille, France, Octobre, 2009.

[23] F. Bergaya and G. Lagaly, "General introduction: clays, clay minerals, and clay science," *Developments in Clay Science*, vol. 5, pp. 1–19, 2013.

[24] G. Crini, "Non-conventional low-cost adsorbents for dye removal: a review," *Bioresource Technology*, vol. 97, no. 9, pp. 1061–1085, 2006.

[25] R. Srinivasan, "Advances in application of natural clay and its composites in removal of biological, organic, and inorganic contaminants from drinking water," *Advances in Materials Science and Engineering*, vol. 2011, Article ID 872531, 17 pages, 2011.

[26] A. Bhatnagar, E. Kumar, and M. Sillanpää, "Fluoride removal from water by adsorption—a review," *Chemical Engineering Journal*, vol. 171, no. 3, pp. 811–840, 2011.

[33] D. Mohapatra, D. Mishra, S. P. Mishra, G. Roy Chaudhury, and R. P. Das, "Use of oxide minerals to abate fluoride from water," *Journal of Colloid and Interface Science*, vol. 275, no. 2, pp. 355–359, 2004.

[34] Y. S. Ho and McKay, "The adsorption of lead (II) ion on peat. Reponse to comment," *Water Research*, vol. 33, pp. 578–584, 1999.

[35] X. Song, Y. Zhang, C. Yan, W. Jiang, and C. Chang, "The Langmuir monolayer adsorption model of organic matter into effective pores in activated carbon," *Journal of Colloid and Interface Science*, vol. 389, no. 1, pp. 213–219, 2013.

[36] W. J. Weber Jr and J. C. Morris, "Kinetics of adsorption on carbon from solution," *Journal of the Sanitary Engineering Division*, vol. 40, pp. 31–60, 1963.

[37] V. K. Gupta, I. Ali, and V. K. Saini, "Defluoridation of wastewaters using waste carbon slurry," *Water Research*, vol. 41, no. 15, pp. 3307–3316, 2007.

[38] C. Aharoni and M. Ungarish, "Kinetics of activated chemisorption. Part 2. Theoretical models," *Journal of the Chemical Society*, vol. 73, no. 3, pp. 456–464, 1977.

[39] A. Ramesh, H. Hasegawa, T. Maki, and K. Ueda, "Adsorption of inorganic and organic arsenic from aqueous solutions by polymeric Al/Fe modified montmorillonite," *Separation and Purification Technology*, vol. 56, no. 1, pp. 90–100, 2007.

[40] W. Li, Z. Meng, Z. Liu, H. Chen, Q. Wu, and S. Xu, "Chromium (VI) characteristics of bentonite under different modification patterns," *Polish Journal of Environmental Studies*, vol. 25, no. 3, pp. 1075–1083, 2016.

[41] K. F. Hayes, C. Papelis, and J. O. Leckie, "Modeling ionic strength effects on anion adsorption at hydrous oxide/solution interfaces," *Journal of Colloid and Interface Science*, vol. 125, no. 2, pp. 717–726, 1988.

ISSN 2356-7171

Physicochemical Properties of Diacetylenic Light Fuel Oil from Congolese Oleaginous Plant Ongokea gore (Hua) Pierre

J. K. Ntumba,1 A. Mulula,1 K. T. Kashishi,1 M. N. Mifundu,1 R. Robiette,2 and K. M. Taba1

1Department of Chemistry, Faculty of Sciences, University of Kinshasa, BP 190, Kinshasa XI, Congo 2 Institute of Condensed Matter and Nanosciences, Universit´ e Catholique de Louvain, Place Louis Pasteur 1 Box L4.01.02, 1348 Louvain-la-Neuve, Belgium

ABSTRACT

Vegetable oil-based fuels are promising alternative fuels for diesel and light fuel engines because of their environmental and economicstrategic advantages. In this study, Ongokea goreoil(OGO)anditsfullyhydrogenatedoilweretransesterifiedbymeansof ethanol in the presence of sodium ethoxide. Fatty acid ethyl esters (FAEE) products were confirmed by 1HNMRandcharacterized by physical-chemical methods in accordance with the ASTM D 6751 and AFNOR M 15-009 specifications for biodiesels and light biofuels. These methods concern determination of color, density, viscosity, flash and pour points, ash, water and sulfur contents, and corrosion on copper. It was found that pure fatty acid ethyl esters of Ongokea gore oil (B100) and its hydrogenated oil (B100H) meet standard requirements for most of the biodiesel characteristics studied. Only the kinematic viscosity and density values were outside recommended biodiesel standard limits which makes them unsuitable for use in diesel engines. In accordance with the AFNOR M 15-009 specifications of light fuels, they can be used in light fuel engines. Physical-chemical properties of B20, a FAEEblend in petrodiesel, are within the limits prescribed for petrodiesel standards. In brief, Ongokea gore seeds, a nonedible and high-oil-producing feedstock, are suitable starting material for production of light biofuel. The latter blends in petrodiesel can be used as fuel in diesel engines.

1. Introduction

Vegetable oils are considered as a long-term promising source of renewable energy because of their potential to solve problems of environmental safety caused by constant dependence of the world on fossil fuels [1–9]. Commonly used fossil fuels such as oil, coal, and natural gas are associated with negative impacts on environment, particularly on global warming [10–12]. In addition, the supply of these nonrenewable energy resources is likely to end in a near future [13–15]. Therefore, the search for renewable energy resources, such as vegetable oils, is strongly encouraged. It was reported that, in diesel engines, vegetable oils can be used directly as a fuel or as a mixture with petrodiesel [16, 17]. Nevertheless, their high viscosity and low fuel atomization in engines lead to an inaccurate fuel-air mixing and inefficient combustion [18–21]. Problem occurs also during the coking in the injector, deposits in the engine, and thickening lubricants during (FAEE) of both *O. gore* oil and its fully hydrogenated oil. Their physicochemical properties have been analyzed according to ASTM D 6751 and AFNOR M 15-009 specifications and their potential use as biofuel in diesel or light fuel engine evaluated. A FAEE blend in petrodiesel, B20 (20 : 80 mixed), has been also prepared and evaluated.

prolonged operating of the engine [22, 23]. Hence, prior to their use as biodiesel, these vegetable oils have to be subjected to a pretreatment, such as transesterification with short alcohols [24–27].

In a previous study, we have shown that seeds of *Ongokea gore* (Hua) Pierre, which contain about 55% of oil (also called isano oil), possess interesting sustainable chemical applications [28]. Major fatty acids in *O. gore* oil contain diacetylenic groups such as isanic acid, bolekic acid, 8-hydroxy-octadeca-13,17-diene-9,11-diynoic acid, 8-hydroxy-octadec-13-ene-9,11-diynoic acid, and octadeca-13,17-diene-9,11-diynoic acid.

Nowadays, the *O. gore* oil has limited application and the natural production of seeds remains underutilized. To the best of our knowledge, there is no report on production of biofuel using isano oil. In this study, *O. gore* oil has been used as a potential source of starting material for light biofuel production. Therefore, we set to prepare fatty acid ethyl ester B100-H, respectively. For comparison purpose, a mixture of 80% of fossil fuel diesel and 20% of B100 was prepared; the latter was called B20.

Proton Nuclear Magnetic Resonance analysis of B100 and B100-H (^{1}H NMR) was carried out to confirm that the above hydrogenation and transesterification reactions took place.

2. Materials and Methods

2.1. Materials. Adam's catalyst ($PtO_2 \cdot H_2O$) and sodium ethoxide (NaOEt) were purchased from Acros and were used without further purification. Analytical grade solvents, ethyl acetate and ethanol, were purchased from VWR.

Dried seeds of *O. gore* were collected from the Eala botanical garden in Mbandaka, Democratic Republic of Congo (DRC). The material was authenticated at the herbarium of INERA (Institut National de Recherches Agronomiques), Department of Biology, Faculty of Sciences, University of Kinshasa, DRC.

2.2. Methods

2.2.1. Extraction of Oil. The oil was obtained from dehulled and milled seeds by solvent extraction process (maceration), using cyclohexane as solvent at room temperature for 48 h, followed by filtration. After filtration, the solvent was removed in a rotary evaporator, to give 55% of a yellow oil.

2.2.2. Hydrogenation of Isano Oil [31]. Isano oil (0.15 gr) and Adam's catalyst (5 mol%) were mixed in ethyl acetate (50 mL). The reaction mixture was purged twice with argon and then 3 times with hydrogen. The mixture was then stirred at room temperature for 48 hours under hydrogen atmosphere (double balloon, 1 atm) and then filtered through celite before being concentrated in a rotary evaporator. A white powder was obtained with a quantitative yield.

2.2.3. Preparation of Ethyl Esters of Isano Oil. Synthesis of ethyl ester of isano oil was carried out by transesterification with sodium ethoxide according to the method of Christie [32]. In a 1 L round-balloon flask (immersed in a temperature controlling silicon oil bath, equipped with a magnetic stirrer, a thermometer, and a condenser with a balloon filled of helium) containing a known amount of ethanol (6 : 1 molar ratio to oil), isano oil and then sodium ethoxide (6 : 1 molar ratio to oil) were added. The reaction mixture was stirred vigorously and heated at 70°C for 1 h. Upon cooling, it separated into two layers. The ester mixture formed the upper layer and glycerin formed the lower layer. Excess ethanol from upper layer was recovered, using a rotary evaporator. Ethyl acetate (30 mL) was then added to the residue, and the resulting solution was washed with water and neutralized with few drops of aqueous HCl 1 N followed by extraction with ethyl acetate (three times). The organic extracts were dried over anhydrous magnesium sulfate, and the solvent was removed under reduced pressure.

The hydrogenated isano oil fatty acid ethyl ester was prepared following similar procedure. Isano oil and its hydrogenated oil fatty acid ethyl ester were named B100 and

^{1}H NMR analysis was recorded on NMR Bruker Avance 500 MHz spectrometers. The chemical shifts were reported in ppm downfield from internal tetramethylsilane (TMS) at $\delta = 0$.

The physicochemical properties of different fuels obtained were determined at the SEP-Congo Society (Kinshasa, D.R. Congo). The physicochemical properties determined according to international standards ASTM D 6751 [33] and AFNOR M 15-009 [29] are color (ASTM D-1500), density (ASTM D-4052), viscosity at 37.8°C and 40°C (ASTM D-445), viscosity at 50°C (NF T 60-100), flash point (ASTM D-93), pour point (ASTM D-97), ash content (ASTM D-482), water content (ASTM D-95), sulfur content (ASTM D-4294), and copper corrosion (ASTM D-130).

3. Results and Discussion

3.1. Transesterification of Oil to FAEE. ^{1}H NMR spectrum of the α-methylene groups of the long-chain ethyl esters should present a signal in the region between 4.00 and 4.40 ppm as quadruplet (characteristic of ethyl esters), while the spectrum of oils showed signals associated with the α-methylene groups of the triacylglycerides (doublet of doublets) [33].

3.1.1. Production of B100. Transesterification process yielded about 80% of Isano oil's FAEE which was attested by a quadruplet at 4.13 ppm ^{1}H NMR, due to methylene hydrogens of the ethyl carbon (C1) neighbors oxygen of the ester (Figure 1(b)). Isano oil's ^{1}H NMR spectrum exhibited signals at 4.14 ppm and 4.30 ppm due to two glycerol hydrogen atoms (Figure 1(a)).

3.1.2. Production of B100-H. The effectiveness of the oil hydrogenation reaction was confirmed by comparing ^{1}H NMR spectra prior to hydrogenation (Figure 1(a)) and after hydrogenation of isano oil (Figure 2).

Vinylic hydrogen atoms located in the region between 4.5 and 6.5 ppm in isano oil's ^{1}H NMR (Figure 1(a)) disappeared in the ^{1}H NMR of the hydrogenated product. Only signals due to the protons of the central glycerol part of tri-, di-, and monoglycerides present in the oil remained (Figure 2).

All triglycerides were converted to ethyl esters. Comparing ^{1}H NMR spectra before and after transesterification of hydrogenated oil (Figures 2 and 3, resp.), one can notice multiplets corresponding to glycerol hydrogen in the region between 4.00 and 4.30 ppm which changed to a quadruplet after reaction in the same region, corresponding to ethyl hydrogen atoms of methylene neighboring oxygen. The presence of signals at 3.55 ppm, 3.66 ppm, and 5.30 ppm (central hydrogen atoms of the glycerol part) could be due to the presence of mono- and/or diglycerides which would be still present in the obtained product.

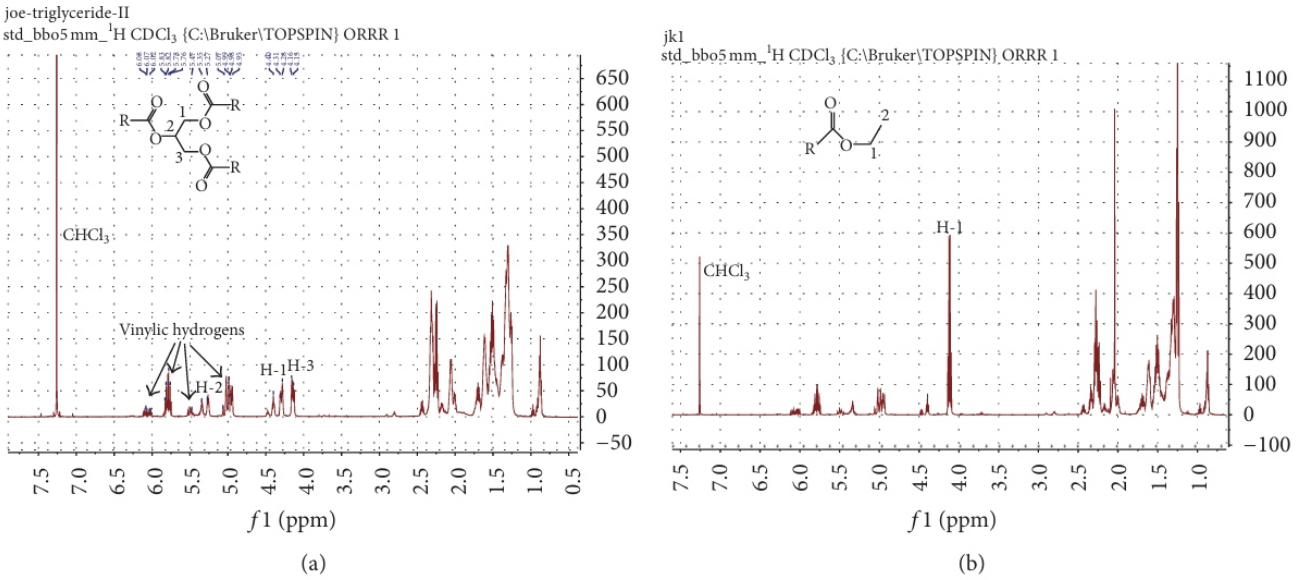

FIGURE 1: ^{1}H NMR: (a) of isano oil and (b) of ethyl ester from isano oil.

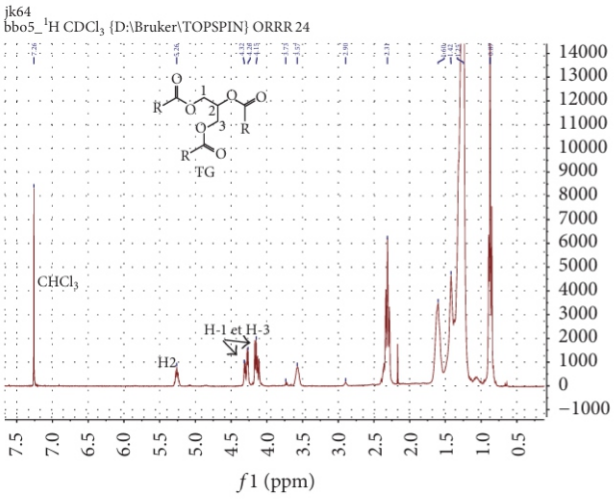

FIGURE 2: ^{1}HNMR of hydrogenated isano oil. TG: triglyceride.

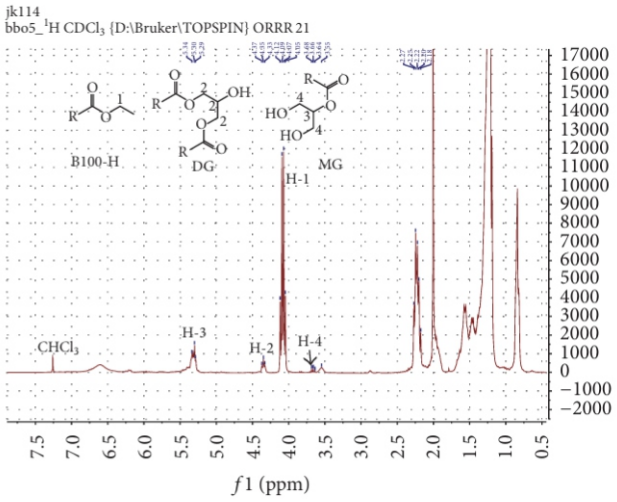

FIGURE 3: ^{1}HNMR of B100-H. DG: diglyceride; MG: monoglyceride.

3.2. Fuel Characterization. The samples were tested to determine the fuel characteristics according to ASTM D 6751 and AFNOR M 15-009 Biodiesel and Light fuel oil Quality Assurance Standard Test. Table 1 summarizes the test methods used, the standards limit as recommended by ASTM D 6751 and AFNOR M 15-009, and our results.

Color has no direct influence on functioning of an engine but just gives an indication of the quality of samples. Indeed, for diesel, the color shows the quality of cracking during the refining of crude oil; it indicates trace pollution from black asphalt products [34]. For vegetable oils, color is due to either the presence of suspended solids or the presence of the pigments that contain oils such as β-carotene.

The density is a basic physical property which can be used (in addition to other properties) to characterize the light and heavy fractions of a fuel. A density in the range $810 < d < 890$ Kg/m^3 ensures good running of engine [34]. In view of our results, *Ongokea gore* oil (OGO), its FAEE B100, and its hydrogenated oil FAEE B100-H have all densities beyond the maximum limit required of 890 Kg/m^3. In their study on ethanolysis of Waste Cooking Oil Ethyl Esters of olive and sunflower oils, Encinar et al. found that the density of FAEE obtained was in accordance with limitation standards [35]. B20 (80% fossil fuel diesel) has logically a lower mass than *O. Gore* oil, B100 and B100-H, and hence a lower density (865 kg/m^3). Since a too dense fuel tends to deplete the fuel mixture in the combustion chamber due to poor fuel atomization by the injectors, causing an increase in particulate emissions (unburned) *O. gore* oil, B100 and B100-H products, will have bigger risk of impoverishment of their fuel mixture as compared to B20 and diesel.

Table 1: Physicochemical properties of GO, OGO, B100, B100-H, and B20.

Properties (units)	Limitations	Gasoil (GO)	*Ongokea gore* oil (OGO)	B100	B100-H	B20	Methods [29, 30]
Yield (%)	—	—	55	80	80	100	—
Color (code)	5,0 max	4,0	4,0	4,0	4,0	4,0	ASTM D-1500
Density at 15°C (Kg/m^3)	810,0–890,0	867,0	965,0	943,0	928,0	865,9	ASTM D-4052
Viscosity at 37,8°C (mm^2/s oucSt)	2,0–6,0	4,11	—	—	—	5,30	ASTM D-445
Viscosity at 40°C (mm^2/s oucSt)	2,0–6,0	4,09	—	—	—	5,22	ASTM D-445
Viscosity at 50°C (mm^2/s or cSt)	≤15	—	—	4,5	3,2	—	AFNOR NF T 60-100
Flash point (°C)	60 min	73	102	88	79	64	ASTM D-93
Pour point (°C)	+5 max	−10	−31	−25	−1	−13	ASTM D-97
Total sulfur (% weight)	0,5 max	0,219	0,025	0,022	0,025	0,140	ASTM D-4294
Ash contents (% masse)	0,01 max	0,01	0,0031	0,0198	0,012	0,0161	ASTM D-482
Water content (% vol)	0,05 max	0,0	0,4	0,0	0,4	0,08	ASTM D-95
Corrosion of Cu (code)	1 max	1a	1a	1a	1a	1a	ASTM D-130

One of the properties to be considered in assessing the overall risk of a fuel flammability is the flash point. This is the highest temperature at which a fuel can be handled without risk of explosion [36]. The flash point is much higher for starting raw oil (102°C). Other less dense products have lighter constituents than those of the oil. Thus, their vapor pressure is higher, making their flashpoint lower (88, 79, and 64°C, corresponding to B100, B100-H, and B20, resp.). However, the flash point observed for B100, B100-H, and B20 (Table 1) meets the ASTM specifications for all biodiesel products. So, as a fuel, they are all expected to be safe during transport and storage.

The pour point of a fuel is the lowest temperature at which fuel freezes. In other words, this is an index of the lowest temperature of its use for certain applications. This value determines the fuel heating conditions to consider in cold weather by appropriate additives [34]. *Ongokea gore* oil is more viscous; thus, it should freeze much slower (−31°C) than its corresponding ethyl esters B100 and B100-H (−25 and −1°C, resp.), which are more fluid. B20 also presents a lower pour point than *Ongokea gore* oil (−13°C). This latter was not purified before use; it thus may be possible that a high content of heavy fraction is responsible for its high viscosity and therefore its high pour point. Maximum permitted sulfur content is fixed at 0.5% by weight. Sulfur compounds are known to cause corrosion of shirts diesel engines and foul odors of diesel exhausts. The use of sulfuric acid in the preparation of biodiesel by acid catalysis may cause, in the case of a noneffective elimination of the acid, deterioration of rubber components and corrosion of parts of metal engine. A base catalysis is therefore recommended.

acid derived from the oxidation of the engine oil or fuel [36]. The test of corrosion on the blade copper is used to control the corrosiveness of fuel toward the copper metal, which is used in diesel engines. According to the standard method, corrosion should not exceed level 1 (light yellow)

The ash components are considered as undesirable impurities or contaminants. These are salts and inorganic oxides that remain in the solid state after complete combustion of the fuel: among them, silicon, iron, calcium, sodium, and vanadium, with the latter representing, in some cases, 50% of the total ash [34]. The specifications provide no measurable traces of ash in the fuel to avoid solid deposits on the cold parts such as valves. In this study, the ash content is within acceptable standards for all tested products.

In itself, water would not be a drawback but it usually contains either dissolved or suspended inorganic matter which may give ash, especially sodium and magnesium chlorides. The water content is thus set to no measurable traces. Moreover, the purification of heavy fuels can be achieved by stirring with water, which dissolves the soluble inorganic matter, followed by centrifugation, which removes the contaminated water and solids suspension [34]. However, in the case of biodiesel, which are ethyl esters, it would be better not to have any water because the presence of residual base or acid would hydrolyze esters into carboxylic acids which undoubtedly wear engine gaskets. A measurable amount of water content was detected in the *Ongokea gore* oil (0.4%), in B100-H (0.4%), and in B20 (0.08%). These values are slightly above the required standard of 0.05%, which would be due to poor drying after aqueous workup during preparation of these fuels.

Corrosion is, with rust, one of the phenomena that lead to an increase in wear and, in extreme cases, to the destruction of certain parts of the machines. Corrosion is caused by the attack of metals by acidic compounds. In diesel engines, these compounds are sulfurous and sulfuric anhydride and sulfuric

4. Conclusion

This study elaborates the use of underutilized, nonedible *O. gore* oil as a starting biomaterial for the production of a high quality light fuel oil.

in a reference scale. In this study, all biodiesels and crude oil have the maximum recommended value of 1. They do not corrode the engine neither during operation nor during storage.

Viscosity was performed at different temperatures: at 37.8°C for conforming to national standards, at 40°C for conforming to ASTM D 445 requirement for diesel fuel oil grade D2, and at 50°C for conforming to ASTM D 445 for diesel fuel oil grade D4 or light fuel oil.

The kinematic viscosity of B20 is 5.30 centistokes at 37.8°C and 5.22 at 40°C. These values are slightly higher than that of diesel fuel at the same temperature, but this is without harmful consequences to the engine because the value obtained is found to be within acceptable limits (2–6 cSt). Regarding *Ongokea gore* oil, B100, and B100-H, their viscosities at 37.8°C or 40°C were not carried to completion because, after 30 minutes of evaluation, analysis was not over, while it took only about 5 minutes for diesel. Obviously, the mobility of the particles is smaller in B100 and B100-H as compared to diesel explaining the lower fluidity and the increase in viscosity. However, this increase makes more difficult fuel atomization and reduces the effectiveness of injectors [34]. These viscosity values obtained certify that FAEE B100 and B100-H have an adverse flow and spray quality for diesel engine and therefore a poor quality of spontaneous combustion. We thus proposed to measure the viscosities of these standard FAEE at 50°C, comparing them to light fuel oil. Indeed, according to French 7 standards AFNOR [30], a light fuel oil is a mixture of hydrocarbons from mineral or synthetic origin, particularly destined for the production of heat in the combustion plants and meeting the following specifications:

(i) Distillation: distillate volume < 65% at 250°C and <85% at 350°C

(ii) Viscosity ≤ 15 cSt at 50°C

(iii) Sulfur content ≤ 2% (w/w)

(iv) Water content ≤ 0.5% (w/w)

(v) Flash point ≥ 70°C

(vi) Pour point ≤ 0°C.

Thus, B100 and B100-H whose viscosities are above 15 cSt at either 37.8°C or 40°C and 4.5 and 3.2 centistokes, respectively, at 50°C are good alternative light fuel oil instead of diesel.

In general, the behavior observed in this work, in relation to color, flash and pour points, ash, water and sulfur contents, and corrosion on copper, agrees with that obtained by other authors [35, 37, 38].

Two different FAEE (fatty acid ethyl esters) and one biodiesel were prepared and analyzed: *O. gore* oil (B100), a biofuel obtained by ethanolic transesterification, B100-H, which is a biofuel produced by transesterification of hydrogenated isano oil, and B20, a mixture of 20% B100 and 80% diesel. These three biofuels have been subjected to physicochemical tests according to international standards ASTM and AFNOR. It should be noted that B20 biodiesel is a fuel of high quality able to replace diesel in a diesel engine because all its physicochemical properties studied (color, density, viscosity, flash point, pour point, ash content, water content, sulfur content, and corrosion on Cu) are in the range of required standards. Since fuel physicochemical properties of B100 and B100-H are of the same order, it is likely that B100-H will be more stable during storage. Both fuels are not effective biodiesels candidate but they can be used as light fuel oil. Thus, FAEE of *Ongokea gore* oil appears to be promising alternative fuel for conventional light biofuel engines. The production of *O. gore* light fuel oil could be an added value to an underutilized agricultural product.

Competing Interests

The authors declare that they have no competing interests.

Acknowledgments

This work was funded by the Commission Universitaire pour le Développement (CUD). This work was conducted in part in Belgium at the Université catholique de Louvain. R. Robiette is a *Chercheur Qualifié* of the Fonds de la Recherche Scientifique (FNRS).

References

[1] J. Xue, T. E. Grift, and A. C. Hansen, "Effect of biodiesel on engine performances and emissions," *Renewable and Sustainable Energy Reviews*, vol. 15, no. 2, pp. 1098–1116, 2011.

[2] L. Li and B. P. Loo, "Alternative and transitional energy sources for urban transportation," *Current Sustainable/Renewable Energy Reports*, vol. 1, no. 1, pp. 19–26, 2014.

[3] L. Lin, Z. Cunshan, S. Vittayapadung, S. Xiangqian, and D. Mingdong, "Opportunities and challenges for biodiesel fuel," *Applied Energy*, vol. 88, no. 4, pp. 1020–1031, 2011.

[4] R. Altin, S. Çetinkaya, and H. S. Yücesu, "Potential of using vegetable oil fuels as fuel for diesel engines," *Energy Conversion and Management*, vol. 42, no. 5, pp. 529–538, 2001.

[5] A. S. Ramadhas, S. Jayaraj, and C. Muraleedharan, "Use of vegetable oils as I.C. engine fuels—a review," *Renewable Energy*, vol. 29, no. 5, pp. 727–742, 2004.

[6] S. S. Sidibé, J. Blin, G. Vaitilingom, and Y. Azoumah, "Use of crude filtered vegetable oil as a fuel in diesel engines state of the art: literature review," *Renewable and Sustainable Energy Reviews*, vol. 14, no. 9, pp. 2748–2759, 2010.

[7] A. B. Chhetri, M. S. Tango, S. M. Budge, K. C. Watts, and M. R. Islam, "Non-edible plant oils as new sources for biodiesel production," *International Journal of Molecular Sciences*, vol. 9, no. 2, pp. 169–180, 2008.

[8] S. P. Singh and D. Singh, "Biodiesel production through the use of different sources and characterization of oils and their esters as the substitute of diesel: a review," *Renewable and Sustainable Energy Reviews*, vol. 14, no. 1, pp. 200–216, 2010.

high free fatty acid oil (waste cooking oil) to biodiesel: a review," *Biotechnology Advances*, vol. 28, no. 4, pp. 500–518, 2010.

[25] I. M. Atadashi, M. K. Aroua, A. R. A. Aziz, and N. M. N. Sulaiman, "Refining technologies for the purification of crude biodiesel," *Applied Energy*, vol. 88, no. 12, pp. 4239–4251, 2011.

[26] J. Zhang, S. Chen, R. Yang, and Y. Yan, "Biodiesel production from vegetable oil using heterogenous acid and alkali catalyst," *Fuel*, vol. 89, no. 10, pp. 2939–2944, 2010.

[9] A. Demirbas, "Progress and recent trends in biodiesel fuels," *Energy Conversion and Management*, vol. 50, no. 1, pp. 14–34, 2009.

[10] T. F. Stocker, D. Qin, G. K. Plattner, M. Tignor, S. K. Allen, and P. M. Midgley, "Climate change Lecture: The physical science basis," 2014.

[11] M. Höök and X. Tang, "Depletion of fossil fuels and anthropogenic climate change—a review," *Energy Policy*, vol. 52, pp. 797–809, 2013.

[12] R. J. Plevin, M. O'Hare, A. D. Jones, M. S. Torn, and H. K. Gibbs, "Greenhouse gas emissions from biofuels' indirect land use change are uncertain but may be much greater than previously estimated," *Environmental Science and Technology*, vol. 44, no. 21, pp. 8015–8021, 2010.

[13] R. E. Dunlap and A. K. Jorgenson, *The Wiley-Blackwell Encyclopedia of Globalization*, Edited by G. Ritzer, Wiley-Blackwell, 1st edition, 2012.

[14] B. R. Singh and O. Singh, "Global trends of fossil fuel reserves and climate change in the 21st century," in *Fossil Fuel and the Environment*, S. Khan, Ed., chapter 8, InTech, Rijeka, Croatia, 2012.

[15] H. Pan, Y.-S. Hu, and L. Chen, "Room-temperature stationary sodium-ion batteries for large-scale electric energy storage," *Energy and Environmental Science*, vol. 6, no. 8, pp. 2338–2360, 2013.

[16] A. Murugesan, C. Umarani, R. Subramanian, and N. Nedunchezhian, "Bio-diesel as an alternative fuel for diesel engines—a review," *Renewable and Sustainable Energy Reviews*, vol. 13, no. 3, pp. 653–662, 2009.

[17] N. Tippayawong, A. Pittayapak, and W. Jompakdee, "Analysis of energy requirement for vegetable oil production in Northern Thailand's farms," *CMU Journal*, vol. 2, pp. 37–47, 2003.

[18] J. Blin, C. Brunschwig, A. Chapuis et al., "Characteristics of vegetable oils for use as fuel in stationary diesel engines—towards specifications for a standard in West Africa," *Renewable and Sustainable Energy Reviews*, vol. 22, pp. 580–597, 2013.

[19] A. S. Ramadhas, S. Jayaraj, and C. Muraleedharan, "Use of vegetable oils as I.C. engine fuels—a review," *Renewable Energy*, vol. 30, pp. 795–803, 2005.

[20] K. Pramanik, "Properties and use of jatropha curcas oil and diesel fuel blends in compression ignition engine," *Renewable Energy*, vol. 28, no. 2, pp. 239–248, 2003.

[21] A. Srivastava and R. Prasad, "Triglycerides-based diesel fuels," *Renewable & Sustainable Energy Reviews*, vol. 4, no. 2, pp. 111–133, 2000.

[22] W. M. Adaileh and K. S. AlQdah, "Performance of diesel engine fuelled by a biodiesel extracted from a waste cocking oil," *Energy Procedia*, vol. 18, pp. 1317–1334, 2012.

[23] T. P. Durrett, C. Benning, and J. Ohlrogge, "Plant triacylglycerols as feedstocks for the production of biofuels," *Plant Journal*, vol. 54, no. 4, pp. 593–607, 2008.

[24] M. K. Lam, K. T. Lee, and A. R. Mohamed, "Homogeneous, heterogeneous and enzymatic catalysis for transesterification of

[27] A. P. Vyas, J. L. Verma, and N. Subrahmanyam, "A review on FAME production processes," *Fuel*, vol. 89, no. 1, pp. 1–9, 2010.

[28] J. K. Ntumba, L. Collard, K. M. Taba, and R. Robiette, "Isolation of a series of fatty acid components of ongokea gore seed (isano) oil and their detailed structural analysis," *Lipids*, vol. 50, no. 3, pp. 313–322, 2015.

[29] Annual Book of ASTM Standards, *Petroleum Products, Lubricants, and Fossil Fuels*, section 5, ASTM International Press, Pennsylvania, Pa, USA, 2010.

[30] AFNOR: Recueil des Normes Françaises, *Produits Pétroliers: Combustibles Liquides*, AFNOR Press, Paris, France, 7th edition, 1988.

[31] B. M. Trost, M. J. Bartlett, A. H. Weiss, A. J. Vonwangelin, and V. S. Chan, "Development of Zn-prophenol-catalyzed asymmetric alkyne addition: synthesis of chiral propargylic alcohols," *Chemistry—A European Journal*, vol. 18, no. 51, pp. 16498–16509, 2012.

[32] W. W. Christie, "Preparation of ester derivatives of fatty acids for chromatographic analysis," in *Advances in Lipid Methodology—Two*, W. W. Christie, Ed., Oily Press, Dundee, UK, 1993.

[33] I. G. Rosset, M. C. H. Tavares, E. M. Assaf, and A. L. M. Porto, "Catalytic ethanolysis of soybean oil with immobilized lipase from Candida antarctica and ^{1}H NMR and GC quantification of the ethyl esters (biodiesel) produced," *Applied Catalysis A: General*, vol. 392, no. 1-2, pp. 136–142, 2011.

[34] P. Wuithier, *Le pétrole: Raffinage et Génie Chimique*, Editions Technip, Paris, France, 1st edition, 1965.

[35] J. M. Encinar, J. F. González, and A. Rodríguez-Reinares, "Ethanolysis of used frying oil. Biodiesel preparation and characterization," *Fuel Processing Technology*, vol. 88, no. 5, pp. 513–522, 2007.

[36] J. Denis, J. Briant, and J. C. Hipeaux, *Physico-Chimie des Lubrifiants, Analyses et Essais*, Editions Technip, Paris, France, 1997.

[37] N. Foidl, G. Foidl, M. Sanchez, M. Mittelbach, and S. Hackel, "*Jatropha curcas* L. as a source for the production of biofuel in Nicaragua," *Bioresource Technology*, vol. 58, no. 1, pp. 77–82, 1996.

[38] L. R. V. Da Conceição, C. E. F. Da Costa, G. N. Da Rocha Filho, E. R. Pereira-Filhob, and J. R. Zamian, "Ethanolysis optimisation of jupati (Raphia taedigera Mart.) oil to biodiesel using response surface methodology," *Journal of the Brazilian Chemical Society*, vol. 26, no. 7, pp. 1321–1330, 2015.

Instructions for Authors

Essentials for Publishing in this Journal

1 Submitted articles should not have been previously published or be currently under consideration for publication elsewhere.

2 Conference papers may only be submitted if the paper has been completely re-written (taken to mean more than 50%) and the author has cleared any necessary permission with the copyright owner if it has been previously copyrighted.

3 All our articles are refereed through a double-blind process.

4 All authors must declare they have read and agreed to the content of the submitted article and must sign a declaration correspond to the originality of the article.

Submission Process

All articles for this journal must be submitted using our online submissions system. http://enrichedpub.com/ . Please use the Submit Your Article link in the Author Service area.

Manuscript Guidelines

The instructions to authors about the article preparation for publication in the Manuscripts are submitted online, through the e-Ur (Electronic editing) system, developed by **Enriched Publications Pvt. Ltd**. The article should contain the abstract with keywords, introduction, body, conclusion, references and the summary in English language (without heading and subheading enumeration). The article length should not exceed 16 pages of A4 paper format.

Title

The title should be informative. It is in both Journal's and author's best interest to use terms suitable. For indexing and word search. If there are no such terms in the title, the author is strongly advised to add a subtitle. The title should be given in English as well. The titles precede the abstract and the summary in an appropriate language.

Letterhead Title

The letterhead title is given at a top of each page for easier identification of article copies in an Electronic form in particular. It contains the author's surname and first name initial .article title, journal title and collation (year, volume, and issue, first and last page). The journal and article titles can be given in a shortened form.

Author's Name

Full name(s) of author(s) should be used. It is advisable to give the middle initial. Names are given in their original form.

Contact Details

The postal address or the e-mail address of the author (usually of the first one if there are more Authors) is given in the footnote at the bottom of the first page.

Type of Articles

Classification of articles is a duty of the editorial staff and is of special importance. Referees and the members of the editorial staff, or section editors, can propose a category, but the editor-in-chief has the sole responsibility for their classification. Journal articles are classified as follows:

Scientific articles:

1. Original scientific paper (giving the previously unpublished results of the author's own research based on management methods).

2. Survey paper (giving an original, detailed and critical view of a research problem or an area to which the author has made a contribution visible through his self-citation);

3. Short or preliminary communication (original management paper of full format but of a smaller extent or of a preliminary character);

4. Scientific critique or forum (discussion on a particular scientific topic, based exclusively on management argumentation) and commentaries. Exceptionally, in particular areas, a scientific paper in the Journal can be in a form of a monograph or a critical edition of scientific data (historical, archival, lexicographic, bibliographic, data survey, etc.) which were unknown or hardly accessible for scientific research.

Professional articles:

1. Professional paper (contribution offering experience useful for improvement of professional practice but not necessarily based on scientific methods);
2. Informative contribution (editorial, commentary, etc.);
3. Review (of a book, software, case study, scientific event, etc.)

Language

The article should be in English. The grammar and style of the article should be of good quality. The systematized text should be without abbreviations (except standard ones). All measurements must be in SI units. The sequence of formulae is denoted in Arabic numerals in parentheses on the right-hand side.

Abstract and Summary

An abstract is a concise informative presentation of the article content for fast and accurate Evaluation of its relevance. It is both in the Editorial Office's and the author's best interest for an abstract to contain terms often used for indexing and article search. The abstract describes the purpose of the study and the methods, outlines the findings and state the conclusions. A 100- to 250-Word abstract should be placed between the title and the keywords with the body text to follow. Besides an abstract are advised to have a summary in English, at the end of the article, after the Reference list. The summary should be structured and long up to 1/10 of the article length (it is more extensive than the abstract).

Keywords

Keywords are terms or phrases showing adequately the article content for indexing and search purposes. They should be allocated heaving in mind widely accepted international sources (index, dictionary or thesaurus), such as the Web of Science keyword list for science in general. The higher their usage frequency is the better. Up to 10 keywords immediately follow the abstract and the summary, in respective languages.

Acknowledgements

The name and the number of the project or programmed within which the article was realized is given in a separate note at the bottom of the first page together with the name of the institution which financially supported the project or programmed.

Tables and Illustrations

All the captions should be in the original language as well as in English, together with the texts in illustrations if possible. Tables are typed in the same style as the text and are denoted by numerals at the top. Photographs and drawings, placed appropriately in the text, should be clear, precise and suitable for reproduction. Drawings should be created in Word or Corel.

Citation in the Text

Citation in the text must be uniform. When citing references in the text, use the reference number set in square brackets from the Reference list at the end of the article.

Footnotes

Footnotes are given at the bottom of the page with the text they refer to. They can contain less relevant details, additional explanations or used sources (e.g. scientific material, manuals). They cannot replace the cited literature.
The article should be accompanied with a cover letter with the information about the author(s): surname, middle initial, first name, and citizen personal number, rank, title, e-mail address, and affiliation address, home address including municipality, phone number in the office and at home (or a mobile phone number). The cover letter should state the type of the article and tell which illustrations are original and which are not.

Notes: